Steel 8622 (8822 Low Side) Carburized Case (Atm.) Iteration #101 and 105

Monotonic Tensile and Fatigue Test Results Including Overload Tests

Prepared by:

J. Lindsey
and
A. Fatemi

Department of Mechanical, Industrial and Manufacturing Engineering
The University of Toledo
Toledo, Ohio 43606

Prepared for:
The AISI Bar Steel Applications Group

September 2009

American Iron and Steel Institute
2000 Town Center, Suite 320
Southfield, Michigan 48075
tel: 248-945-4777
fax: 248-352-1740
www.autosteel.org

TABLE OF CONTENTS

NOMENCLATURE

A_o, A_f	initial, final area	S	engineering stress
HB, HRB, HRC	Brinell, Rockwell B-Scale, Rockwell C-Scale Hardness number	YS, UYS, LYS, YS'	Monotonic yield, upper yield, lower yield, cyclic yield strength
b, c, n	fatigue strength, fatigue ductility, strain hardening exponent	YPE	yield point elongation
D_o, D_f	initial, final diameter	S_u	ultimate tensile strength
e	engineering strain	%EL	percent elongation
E, E'	monotonic, midlife cycle modulus of elasticity	%RA	percent reduction in area
K, K'	monotonic, cyclic strength coefficient	σ, σ_f, σ_f'	true stress, true fracture strength, fatigue strength coefficient
L_o, L_f	initial, final gage length	σ_a, σ_m, $\Delta\sigma$	stress amplitude, mean stress, stress range
$N_{50\%}$, $(N_f)_{10\%}$, $(N_f)_{50\%}$,	number of cycles to midlife, 10% load drop, 50% load drop,	ε_e, ε_p, ε	true elastic, plastic, total strain
$2N_f$	reversals to failure	ε_f, ε_f'	true fracture ductility, fatigue ductility coefficient
P_f, P_u	fracture, ultimate load	ε_a, ε_m, $\Delta\varepsilon$	strain amplitude, mean strain, strain range
R	strain ratio, neck radius	$\Delta\varepsilon_e$, $\Delta\varepsilon_p$	elastic, plastic strain range

NOMENCLATURE

$\sigma_{m,\,SC}$	small cycle mean stress,	$\sigma_{a,\,SC}$	small cycle stress amplitude,
$\sigma_{m,\,OL}$	overload cycle mean stress	$\sigma_{a,\,OL}$	overload cycle stress amplitude
$\varepsilon_{a,\,SC}$	small cycle strain amplitude	$(\Delta\varepsilon_p/2)_{SC}$	small cycle plastic strain amplitude,
$\varepsilon_{a,\,OL}$	overload cycle strain amplitude	$(\Delta\varepsilon_p/2)_{OL}$	overload plastic strain amplitude
$\varepsilon_{m,\,SC}$	small cycle mean strain	B, B_f	number of blocks in a periodic overload test, number of blocks to failure in a periodic overload test
N_{SC}, $N_{f,\,SC(eq)}$	number of small cycles in an overload block, calculated equivalent life of the small cycles in an overload test	$N_{f,\,OL}$	Constant amplitude life to failure at the strain amplitude used for the periodic overload cycle amplitude

UNIT CONVERSION TABLE

Measure	SI Unit	US Unit	from SI to US	from US to SI
Length	mm	in	1 mm = 0.03937 in	1 in = 25.4 mm
Area	mm^2	in^2	1 mm^2 = 0.00155 in^2	1 in^2 = 645.16 mm^2
Load	kN	klb	1kN = 0.2248 klb	1 klb = 4.448 kN
Stress	MPa	ksi	1 MPa = 0.14503 ksi	1 ksi = 6.895 MPa
Temperature	°C	°F	°C = (°F - 32)/1.8	°F = (°C * 1.8) + 32

In SI Unit:

1 kN = 10^3 N 1 Pa = 1 N/m^2 1 MPa = 10^6 Pa = 1 N/mm^2 1 Gpa = 10^9 Pa

In US Unit:

1 klb = 10^3 lb 1 psi = 1 lb/in^2 1 ksi = 10^3 psi

SUMMARY

Monotonic tensile properties and fatigue behavior data were obtained for steel material of iterations 101 and 105. The material was provided by AISI. Two tensile tests were performed to acquire the desired monotonic properties. Both tests gave similar results. Twelve strain-controlled fatigue tests were performed to obtain the fatigue life and cyclic deformation curves and properties. The experimental procedure followed and results obtained are presented and discussed in this report. Periodic overload fatigue behavior and data were also obtained from twelve load-controlled periodic overload fatigue tests. The experimental procedure followed and results obtained from periodic overload tests are also presented and discussed in this report.

I. EXPERIMENTAL PROGRAM

1.1 Material and Specimen Fabrication

1.1.1 Material

The steel material was provided by AISI. The specimens have been prepared from 8822 steel with low side hardenability. The sample has been through carburized in the gage section by austenitizing at 1700F with a 0.9% carbon potential prior to quenching in 150F oil and then tempering at 425F to an aim hardness of 58-60 HRC (see Appendix B). Intergranular oxidation and microstructure of the material are shown in Figures 1 and 2, respectively.

1.1.2 Specimen

In this study, identical round specimens were used for monotonic and fatigue tests. The specimen configuration and dimensions are shown in Figure 3. This configuration deviates slightly from the specimens recommended by ASTM Standard E606 [1]. The recommended specimens have uniform gage sections. The specimen geometry shown in Figure 3 differs by using a large secondary radius in the gage section to compensate for the slight stress concentration at the gage to grip section transition.

All specimens were machined in the Mechanical, Industrial, and Manufacturing Engineering Machine Shop at the University of Toledo. The specimens were initially turned on a lathe to an appropriate diameter for insertion into a CNC/milling machine. Using the CNC machine, final turning was performed to achieve the tolerable dimensions specified on the specimen drawings.

The specimens were then polished prior to testing at the University of Toledo. A commercial round-specimen polishing machine was used to polish the specimen gage section. Three different grits of aluminum oxide lapping film 30 μm, 12 μm, and 3 μm were used. Polishing marks coincided with the longitudinal direction of the specimen. The polished surfaces were carefully examined under magnification to ensure complete removal of machine marks within the test section.

1.2 Testing Equipment

1.2.1 Apparatus

An INSTRON 8801 closed-loop servo-controlled hydraulic axial load frame in conjunction with a Fast-Track digital servo-controller was used to conduct the tests. The load cell used had a capacity of 50 kN. Hydraulically operated grips using universal tapered collets were employed to secure the specimens' ends in series with the load cell.

Total strain was controlled using an extensometer rated as ASTM class B1 [2]. The calibration of the extensometer was verified using displacement apparatus containing a micrometer barrel in divisions of 0.0001 in. The extensometer had a gage length of 0.30 in. and was capable of measuring strains up to 15 %.

In order to protect the specimens' surface from the knife-edges of the extensometer, ASTM Standard E606 recommends the use of transparent tape or epoxy to 'cushion' the attachment. For this study, it was found that application of transparent tape strips was difficult due to the size of the test section. Therefore, epoxy was considered to be the best protection. The tests were performed using M-coat D.

1.2.2 Alignment

Significant effort was put forth to align the load train (load cell, grips, specimen, and actuator). Misalignment can result from both tilt and offset between the central lines of the load train components. In order to align the machine, a round strain-gage bar with two arrays of four strain gages per array that were arranged at the upper and lower ends of the uniform gage section was used. This was done in accordance with ASTM Standard E1012 [3].

1.3 Test Methods and Procedures

1.3.1 Monotonic tension tests

Monotonic tests in this study were performed using test methods specified by ASTM Standard E8 [4]. Two specimens were used to obtain the monotonic properties.

INSTRON Bluehill software was used for the monotonic tests. For the test a strain rate of 0.0025 in/in/min was chosen. This strain rate was three-quarters of the maximum allowable rate specified by ASTM Standard E8 for the initial yield region.

After the tension tests were concluded, the broken specimens were carefully reassembled. The final gage lengths of the fractured specimens were measured with a Vernier caliper having divisions of 0.001 in. Using an optical comparator with 10X magnification and divisions of 0.001 in, the final diameter was measured. It should be noted that prior to the test, the initial diameter was measured with this same instrument.

1.3.2 Constant amplitude fatigue tests

All constant amplitude fatigue tests in this study were performed according to ASTM Standard E606. It is recommended by this standard that at least 10 specimens be used to generate the fatigue properties. For this study, 12 specimens at 4 different strain amplitudes ranging from 0.300% to 0.500% were utilized. INSTRON LCF software was used in all strain-controlled tests. During each strain-controlled test, the total strain was recorded using the extensometer output. Test data were automatically recorded throughout each test.

There were two control modes used for these tests. Strain control was used in all tests with plastic deformation. For one of the elastic tests, strain control was used initially to determine the stabilized load, then load control was used for the remainder of the test and for the rest of the elastic tests, load control was used throughout. The reason for the change in control mode was due to the frequency limitation on the extensometer. For the strain-controlled tests, the applied frequencies ranged from 1 Hz to 1.3 Hz in order to keep a strain rate about 0.02 in/in/sec. For the load-controlled tests, load waveforms with frequencies of up to 24 Hz were used in order to shorten the overall test duration. All tests were conducted using a triangular waveform except the tests run at 24 Hz, when a sinusoidal waveform was used.

1.3.3 Periodic overload fatigue tests

The overload tests were conducted to investigate the effects of periodic overloads on the fatigue life of smaller subsequent cycles. For this study, 12 specimens were tested at 8 different strain amplitudes. The periodic overload tests were run in load control with INSTRON WAVERUNNER software. During each load-controlled test, the total load

was recorded using the load cell output. Test data were automatically recorded throughout each test

The input signal consisted of a periodic fully reversed overload of the type shown in Figure 13. The load history in these tests consisted of repeated load blocks made up of one fully-reversed overload cycle followed by a group of smaller constant amplitude cycles having the same maximum stress as the overload cycle. The overload cycles were applied at frequent intervals to maintain a low crack opening stress resulting in the subsequent cycles being fully open.

With this overload history, as the large cycles become more frequent, the fraction of the total damage done by them increases and that done by the small cycles decreases. The fully reversed strain amplitude for the overload cycle corresponded to 10^4 cycles to failure. The number of small cycles per block, N_{sc}, were adjusted so that they cause 80 to 90% of the damage per block. Small cycle strain levels were selected at or below the run out level of the constant amplitude tests. Small cycles strain amplitudes were used from 0.300% to 0.050% and the number of small cycles per overload cycle ranged between 50 and 300.

II. Experimental results and analysis

2.1 Microstructural Data

A specimen was sectioned longitudinally from the grip end and transversely from the gage section to obtain a general microstructure description. The mounted sample was reground and polished. The sample was examined using light microscopy. The surface of the sample contained roughly 28 microns of intergranular oxidation. The sample was then etched with 3% nital and was reexamined. The microstructure of the case was tempered martensite with retained austenite. The amount of retained austenite was estimated to be 9.1% using image analysis. The microstructure of the core was tempered martensite (see Appendix B). The chemistry of the material is presented in Table 1. Figure 1 shows the inter-granular oxidation in the steel and Figure 2 shows a high magnification view of the microstructure from the gage area. The complete material report for this steel was provided by the Chrysler Materials Engineering Lab and is attached as Appendix B of this report.

2.2 Monotonic Deformation Behavior

The properties determined from monotonic tests are the following: modulus of elasticity (E), yield strength (YS), ultimate tensile strength (S_u), percent elongation (%EL), percent reduction in area (%RA), true fracture strength (σ_f), true fracture ductility (ε_f), strength coefficient (K), and strain hardening exponent (n).

True stress (σ), true strain (ε), and true plastic strain (ε_p) were calculated from engineering stress (S) and engineering strain (e), according to the following relationships which are based on constant volume assumption:

$$\sigma = S(1+e) \tag{1a}$$

$$\varepsilon = \ln(1+e) \tag{1b}$$

$$\varepsilon_p = \varepsilon - \varepsilon_e = \varepsilon - \frac{\sigma}{E} \tag{1c}$$

The true stress (σ) - true strain (ε) plot is often represented by the Ramberg-Osgood equation:

$$\varepsilon = \varepsilon_e + \varepsilon_p = \frac{\sigma}{E} + \left(\frac{\sigma}{K}\right)^{\frac{1}{n}} \tag{2}$$

The strength coefficient, K, and strain hardening exponent, n, are the intercept and slope of the best line fit to true stress (σ) versus true plastic strain (ε_p) data in log-log scale:

$$\sigma = K\left(\varepsilon_p\right)^n \tag{3}$$

In accordance with ASTM Standard E739 [5], when performing the least squares fit, the true plastic strain (ε_p) was the independent variable and the true stress (σ) was the dependent variable. These plots for the two tests conducted are shown in Figure 4. To generate the K and n values, the range of data used in this figure was chosen according to the definition of discontinuous yielding specified in ASTM Standard E646 [6]. Therefore, the valid data range occurred between the end of yield point extension and the strain at maximum load.

The true fracture strength was calculated from

$$\sigma_f = \frac{P_f}{A_f} \tag{4}$$

where P_f is load at fracture and A_f is the area at fracture.

The true fracture ductility, ε_f, is calculated from the relationship based on constant volume:

$$\varepsilon_f = \ln\left(\frac{A_o}{A_f}\right) = \ln\left(\frac{1}{1 - RA}\right) \tag{5}$$

where A_f is the cross-sectional area at fracture, A_o is the original cross-sectional area, and RA is the reduction in area.

A summary of the monotonic properties for this material is provided in Table A.1. The monotonic stress-strain curves are shown in Figure 5. As can be seen from this figure, the two curves are relatively close to each other. For this material, due to the brittleness, fracture occurred before a defined yield point could be reach. Due to this, there was no discernable change in the cross sectional area or the gage length after fracture. This resulted in an inability to define the yield strength, percent elongation, percent reduction in area and true fracture ductility. Refer to Table A.1 for a summary of the monotonic test results.

2.3 Cyclic Deformation Behavior

2.3.1 Transient cyclic response

Transient cyclic response describes the process of cyclic-induced change in deformation resistance of a material. Data obtained from constant amplitude strain-controlled fatigue tests were used to determine this response. Plots of stress amplitude variation versus applied number of cycles can indicate the degree of transient cyclic softening/hardening. Also, these plots show when cyclic stabilization occurs. A composite plot of the transient cyclic response for the steel studied is shown in Figure A.1. The transient response was normalized on the rectangular plot in Figure A.1a, while a semi-log plot is shown in Figure A.1b. Even though multiple tests were conducted at each strain amplitude, data from one test at each strain amplitude tested are shown in these plots.

2.3.2 Steady-state cyclic deformation

Another cyclic behavior of interest was the steady state or stable response. Data obtained from constant amplitude strain-controlled fatigue tests were also used to determine this response. The properties determined from the steady-state hysteresis loops were the following: cyclic modulus of elasticity (E'), cyclic strength coefficient (K'), cyclic strain hardening exponent (n'), and cyclic yield strength (YS'). Half-life (midlife) hysteresis loops and data were used to obtain the stable cyclic properties.

Similar to monotonic behavior, the cyclic true stress-strain behavior can be characterized by the Ramberg-Osgood type equation:

$$\frac{\Delta\varepsilon}{2} = \frac{\Delta\varepsilon_e}{2} + \frac{\Delta\varepsilon_p}{2} = \frac{\Delta\sigma}{2E} + \left(\frac{\Delta\sigma}{2K'}\right)^{\frac{1}{n'}} \quad (6)$$

It should be noted that in Equation 6 and the other equations that follow, E is the average modulus of elasticity that was calculated from the monotonic tests.

The cyclic strength coefficient, K', and cyclic strain hardening exponent, n', are the intercept and slope of the best line fit to true stress amplitude ($\Delta\sigma/2$) versus true plastic strain amplitude ($\Delta\varepsilon_p/2$) data in log-log scale:

$$\frac{\Delta\sigma}{2} = K'\left(\frac{\Delta\varepsilon_p}{2}\right)^{n'} \quad (7)$$

In accordance with ASTM Standard E739 [5], when performing the least squares fit, the true plastic strain amplitude ($\Delta\varepsilon_p/2$) was the independent variable and the stress amplitude ($\Delta\sigma/2$) was the dependent variable. The true plastic strain amplitude was calculated by the following equation:

$$\frac{\Delta\varepsilon_p}{2} = \frac{\Delta\varepsilon}{2} - \frac{\Delta\sigma}{2E} \quad (8)$$

This plot is shown in Figure 6. To generate the K' and n' values, the range of data used in this figure was chosen for $\left[\frac{\Delta\varepsilon_p}{2}\right]_{calculated} \geq 0.0001$ in/in.

The cyclic stress-strain curve reflects the resistance of a material to cyclic deformation and can be vastly different from the monotonic stress-strain curve. The cyclic stress-strain curve is shown in Figure 7. In Figure 8, superimposed plots of monotonic and cyclic curves are shown. Figure A.2 shows a composite plot of the steady-state (midlife) hysteresis loops. Even though multiple tests were conducted at each strain

amplitude, the stable loops from only one test at each strain amplitude are shown in this plot.

2.4 Constant Amplitude Fatigue Behavior

Constant amplitude strain-controlled fatigue tests were performed to determine the strain-life curve. The following equation relates the true strain amplitude to the fatigue life:

$$\frac{\Delta\varepsilon}{2}=\frac{\Delta\varepsilon_e}{2}+\frac{\Delta\varepsilon_p}{2}=\frac{\sigma_f'}{E}(2N_f)^b+\varepsilon_f'(2N_f)^c \qquad (9)$$

where σ_f' is the fatigue strength coefficient, b is the fatigue strength exponent, ε_f' is the fatigue ductility coefficient, c is the fatigue ductility exponent, E is the monotonic modulus of elasticity, and $2N_f$ is the number of reversals to failure.

The fatigue strength coefficient, σ_f', and fatigue strength exponent, b, are the intercept and slope of the best line fit to true stress amplitude ($\Delta\sigma/2$) versus reversals to failure ($2N_f$) data in log-log scale:

$$\frac{\Delta\sigma}{2}=\sigma_f'(2N_f)^b \qquad (10)$$

In accordance with ASTM Standard E739, when performing the least squares fit, the stress amplitude ($\Delta\sigma/2$) was the independent variable and the reversals to failure ($2N_f$) was the dependent variable. This plot is shown in Figure 9. To generate the σ_f' and b values, all data, with the exception of the run-out tests, in the stress-life figure was used.

The fatigue ductility coefficient, ε_f', and fatigue ductility exponent, c, are the intercept and slope of the best line fit to calculated true plastic strain amplitude ($\Delta\varepsilon_p/2$) versus reversals to failure ($2N_f$) data in log-log scale:

$$\left(\frac{\Delta\varepsilon_p}{2}\right)_{calculated} = \varepsilon_f'(2N_f)^c \qquad (11)$$

In accordance with ASTM Standard E739, when performing the least squares fit, the calculated true plastic strain amplitude ($\Delta\varepsilon_p/2$) was the independent variable and the reversals to failure ($2N_f$) was the dependent variable. The calculated true plastic strain amplitude was determined from Equation 8. This plot is shown in Figure 10. To generate the ε_f' and c values, the range of data used in this figure was chosen for $\left[\frac{\Delta\varepsilon_p}{2}\right]_{calculated} \geq 0.0001$ in/in.

The true strain amplitude versus reversals to failure plot is shown in Figure 11. This plot displays the strain-life curve (Eqn. 9) and superimposed fatigue data. A summary of the cyclic properties for this steel is provided in Table 2. Table A.2 provides the summary of the fatigue test results.

A parameter often used to characterize fatigue behavior at stress concentrations, such as at the root of a notch, is Neuber parameter [7]. Neuber's stress range is given by:

$$\sqrt{(\Delta\varepsilon)(\Delta\sigma)E} = 2\sqrt{(\sigma_f')^2(2N_f)^{2b} + \sigma_f'\varepsilon_f'E(2N_f)^{b+c}} \qquad (12)$$

A plot of Neuber stress range versus reversals to failure is shown in Figure 12. This figure displays the Neuber curve based on Eqn. 12 and superimposed fatigue data for this material

2.5 Periodic Overload Fatigue Behavior

Periodic Overload strain-controlled fatigue tests were performed to determine the effective strain-life curve. The effective strain-life curve is plotted using the strain amplitude of the small cycles in the overload block and the calculated equivalent life. The equivalent fatigue lives for the smaller cycles were obtained using the linear damage rule:

$$\frac{N_{OL}}{N_{f,OL}} + \frac{N_{SC}}{N_{f,SC(eq)}} = 1 \qquad (13)$$

where N_{OL} is the number of overload cycles in a periodic overload test, $N_{f,OL}$ is the number of cycles to failure if only overloads were applied in a test, N_{SC} is the number of smaller cycles in a periodic overload test, and $N_{f,SC(eq)}$ is the computed equivalent fatigue life for the smaller cycles.

The linear damage rule was also used to calculate the cumulative damage of the overload cycles, D_{OL}, as

$$\frac{N_{OL}}{N_{f,OL}} = D_{OL} \qquad (14)$$

Figure 14 shows the effective strain-life data superimposed on the constant amplitude strain life plot. Table A.3 presents a summary of the periodic overload test results.

A plot of the SWT parameter for both the constant amplitude and overload data provides another method of comparison between the two sets of data, where the mean stress present in the small cycles is taken into account. The SWT parameter is given by

$$\sigma_{\max}\varepsilon_a = \frac{1}{E}[(\sigma_f')^2(2N_f)^{2b} + \sigma_f'\varepsilon_f' E(2N_f)^{b+c}] \qquad (15)$$

where $\sigma_{max} = \sigma_m + \sigma_a$. The SWT plot is shown in Figure 15. As in the constant amplitude strain-life curve, the overload data and effective strain-life curve diverged from the constant amplitude curve.

Table 1: Chemical Composition of 8622 (8822 Low Side) Steel (Courtesy of Chrysler)

Element	Wt. %
Carbon, C	0.210%
Manganese, Mn	0.810%
Phosphorus, P	0.020%
Sulfur, S	0.026%
Silicon, Si	0.260%
Chromium, Cr	0.500%
Aluminum, Al	0.031%
Nickel, Ni	0.460%
Molybdenum, Mo	0.250%
Copper, Cu	0.180%
Tin, Sn	0.010%
Vanadium, V	0.005%
Niobium, Nb	0.002%
Dl	2.260%

Table 2: Summary of the Mechanical Properties

Microstructural Data	Average
ASTM grain size number (MAG=500X):	
First longitudinal direction (L-T)	Fine grain 5 - 8
Inclusion rating number (MAG=100x): (Provided by Macsteel Company)	
Type A (sulfide type), thin series	-
Type B (alumina type), thin & heavy series	-
Type C (silicate type, thin & heavy series	-
Type D (globular type), thin & heavy series	-
Hardness:	
Brinell (HB)(converted)	
the first longitudinal direction	-
Transverse direction	615
Rockwell B-scale (HRB)	
The first longgitudinal direction	-
Transverse direction	-
Rockwell C-scale (HRC)(measured)	
The first longgitudinal direction	-
Transverse direction	58
Microstructure type:	
The first longitudinal direction	Tempered martensite
Transverse direction	

Monotonic Properties	Average		Range					
Modulus of elasticity, E, GPa (ksi):	214.7	(31,131)	214.7	-	214.6	(31,139)	-	(31,124)
Yield strength (0.2% offset), YS , MPa (ksi):	-	-	-	-	-	-	-	-
Upper yield strength UYS, MPa (ksi):	-	-	-	-	-	-	-	-
Lower yield strength LYS, MPa (ksi):	-	-	-	-	-	-	-	-
Yield point elongation, YPE (%):	-	-	-	-	-	-	-	-
Ultimate strength, S_u , MPa (ksi):	-	-	-	-	-	-	-	-
Percent elongation, %EL (%):	-		-	-	-			
Percent reduction in area, %RA (%):	-		-	-	-			
Strength coefficient, K , MPa (ksi):	1,864.5	(270.4)	1,778.2	-	1,950.7	(257.9	-	282.9)
Strain hardening exponent, n:	0.0716		0.0624	-	0.0807			
True fracture strength, σ_f , MPa (ksi):	1082.2	(157.0)	1074.6	-	1089.7	(155.9	-	158.0)
True fracture ductility, ε_f (%):	-		-	-	-			

Cyclic Properties	Average		Range					
Cyclic modulus of elasticity, E' , GPa (ksi):	202.7	(29,399)	203.7	-	200.9	(29,546)	-	(29,141)
Fatigue strength coefficient, σ_f' , MPa (ksi):	2,115.0	(306.7)						
Fatigue strength exponent, b:	-0.0962							
Fatigue ductility coefficient, ε_f' :	0.001							
Fatigue ductility exponent, c:	-0.1318							
Cyclic strength coefficient, K' , MPa (ksi):	-							
Cyclic strain hardening exponent, n':	0.8286							
Cyclic yield strength, YS', MPa (ksi)	-							
Fatigue Limit (defined at 10^6 cycles), Mpa (ksi)	523.7	(76.0)						

Some properties (YS, S_u, %EL, %RA, K') could not be measured due to material brittleness

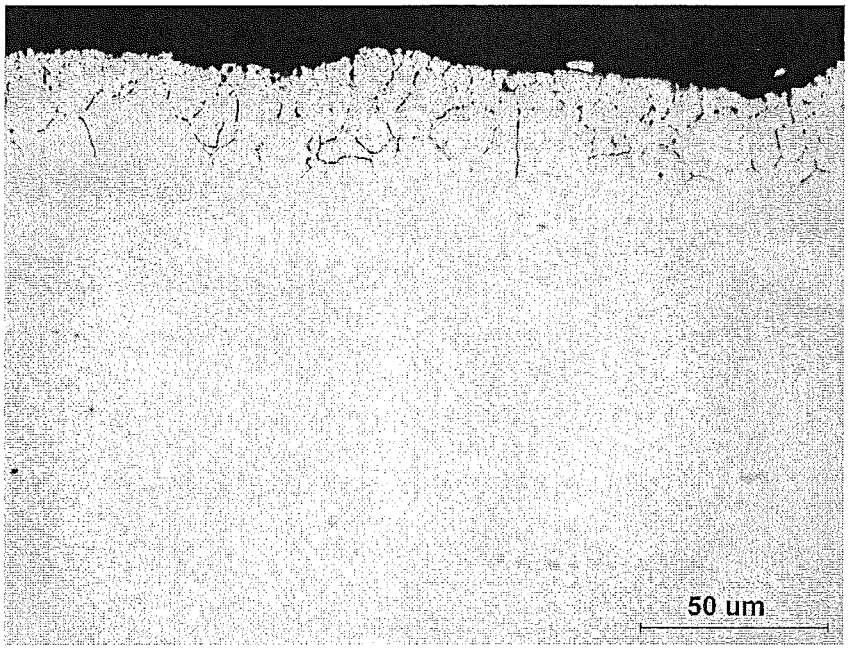

Figure 1: Image of the surface of the grip end in the unetched condition showing the intergranular oxidation. (Courtesy of Chyrsler)

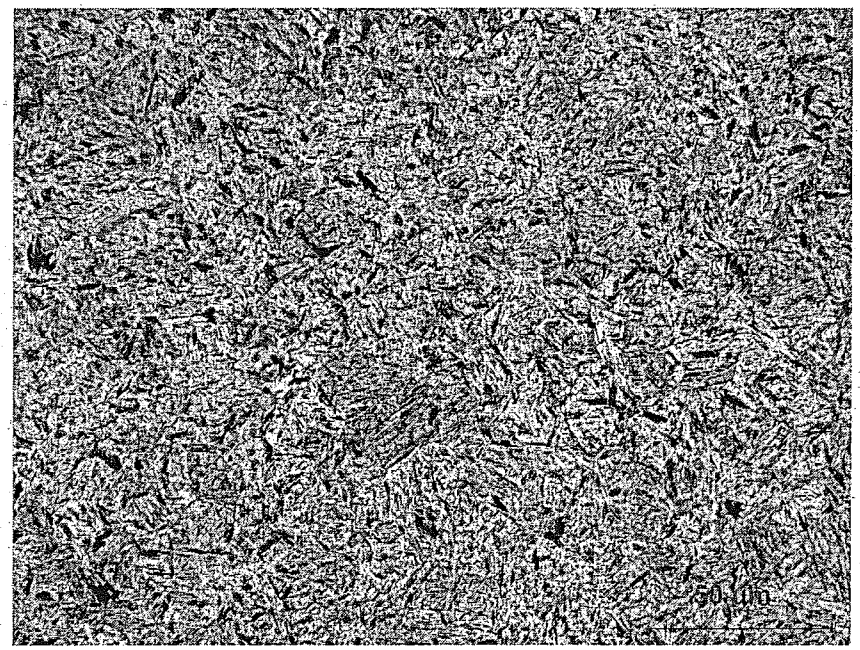
Figure 2: High magnification photo showing the microstructure of the transverse section from the gage area. (Courtesy of Chyrsler)

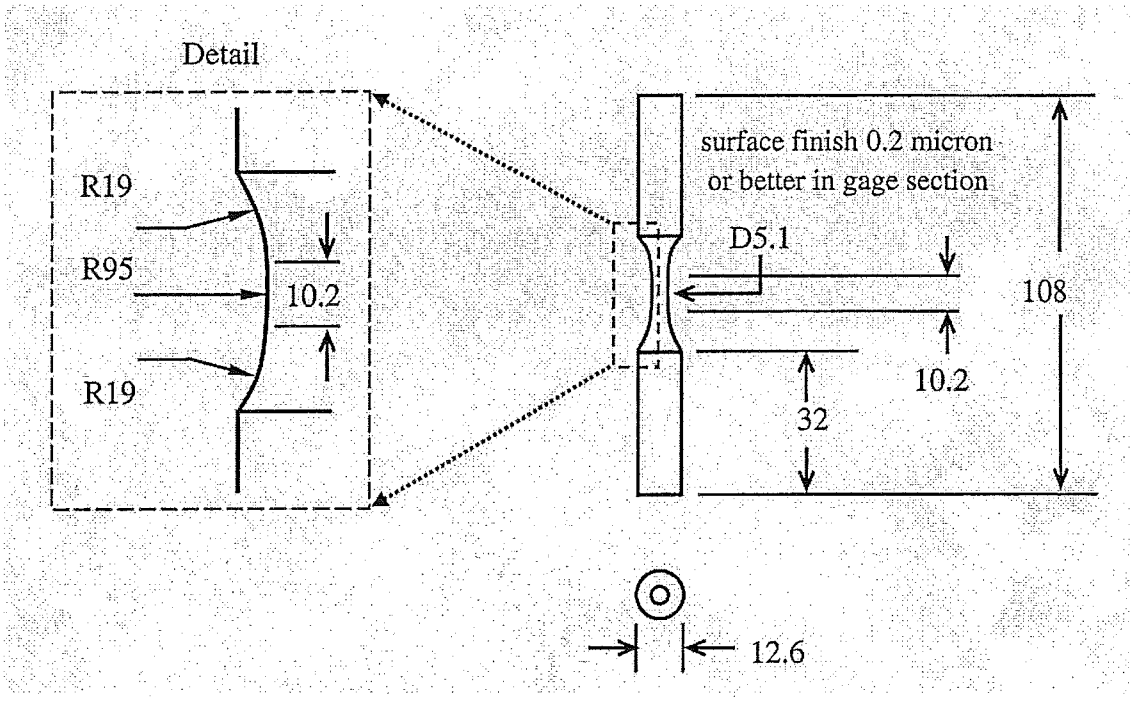

Figure 3: Specimen configuration and dimensions (mm)

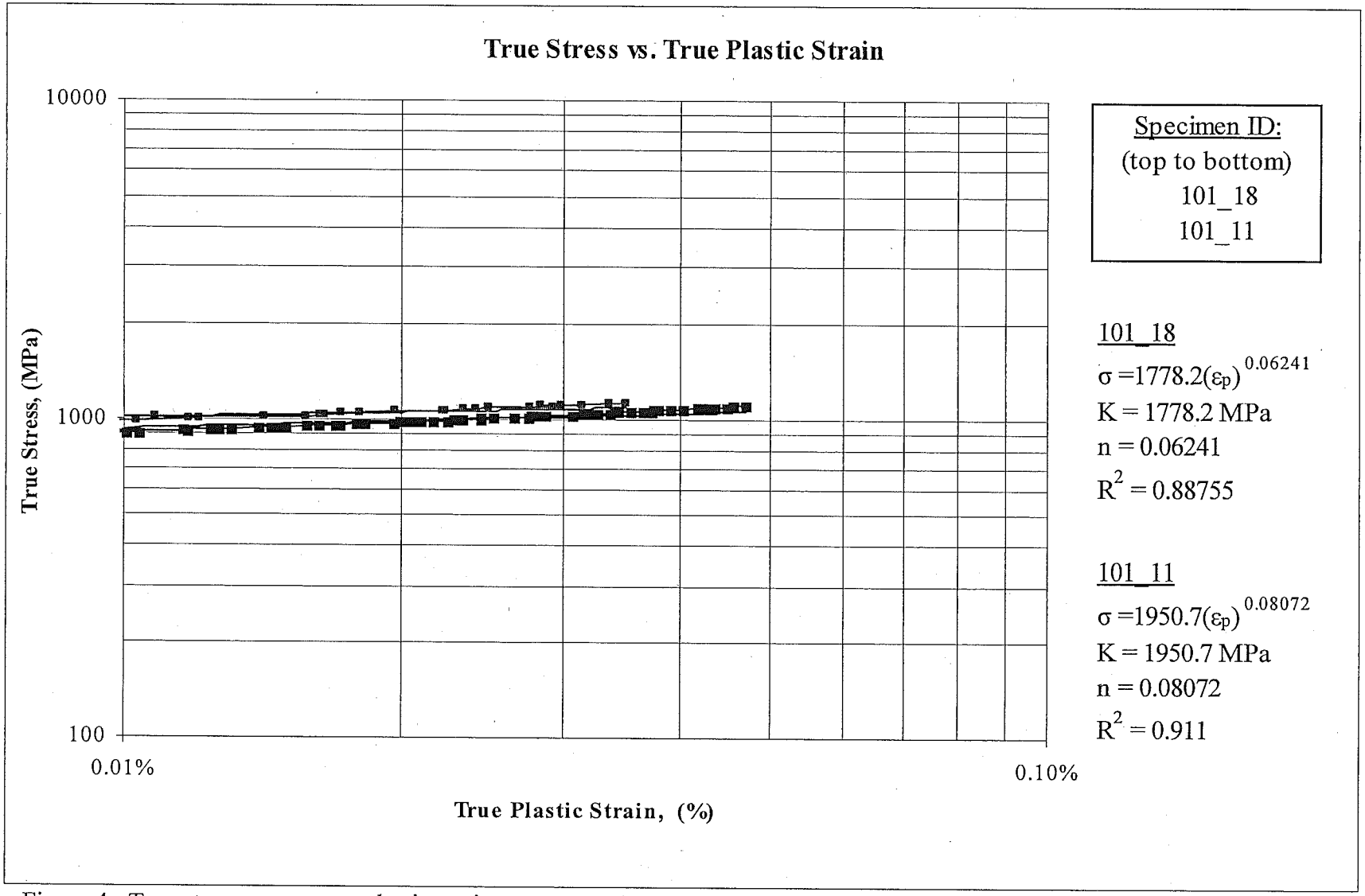

Figure 4: True stress versus true plastic strain

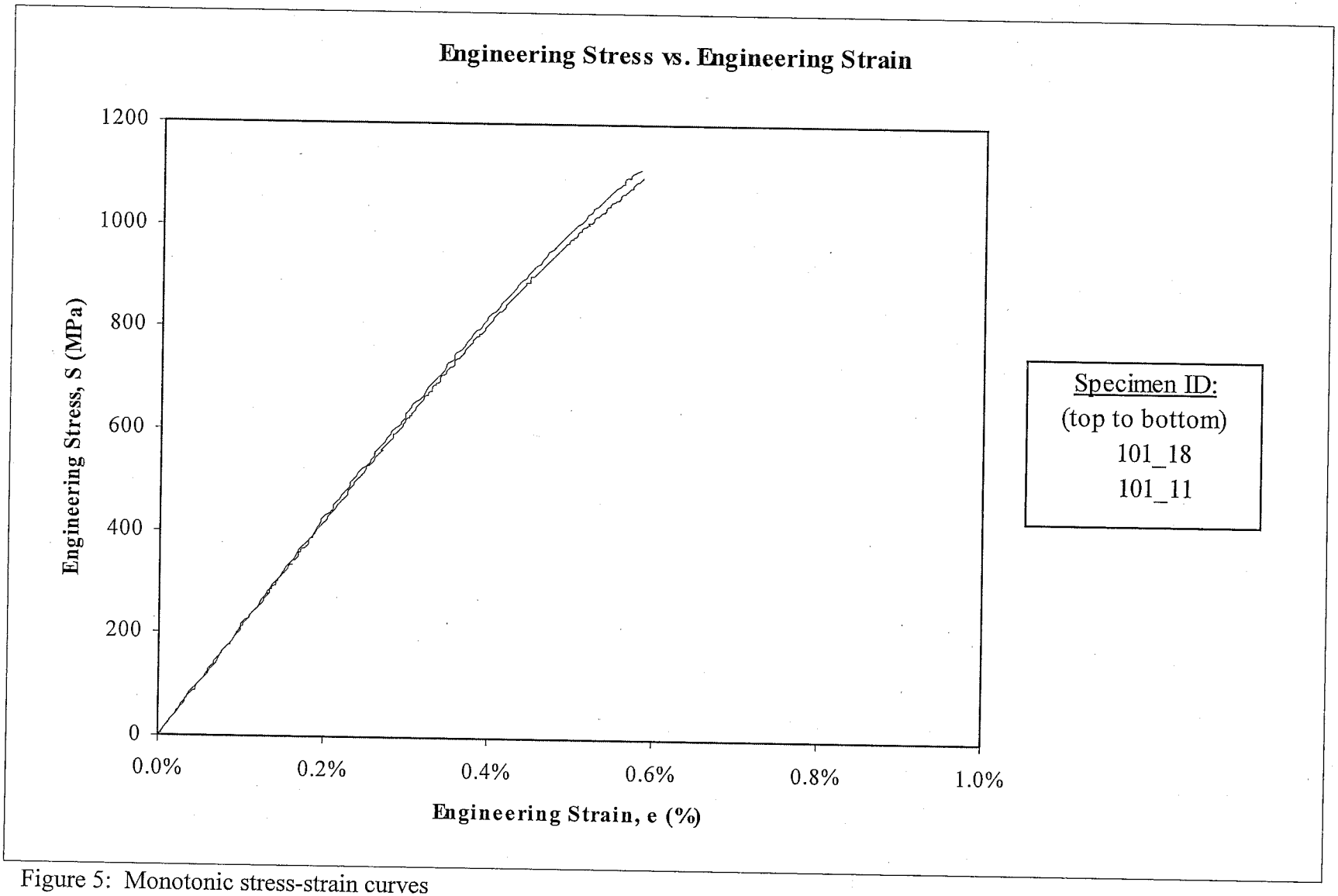

Figure 5: Monotonic stress-strain curves

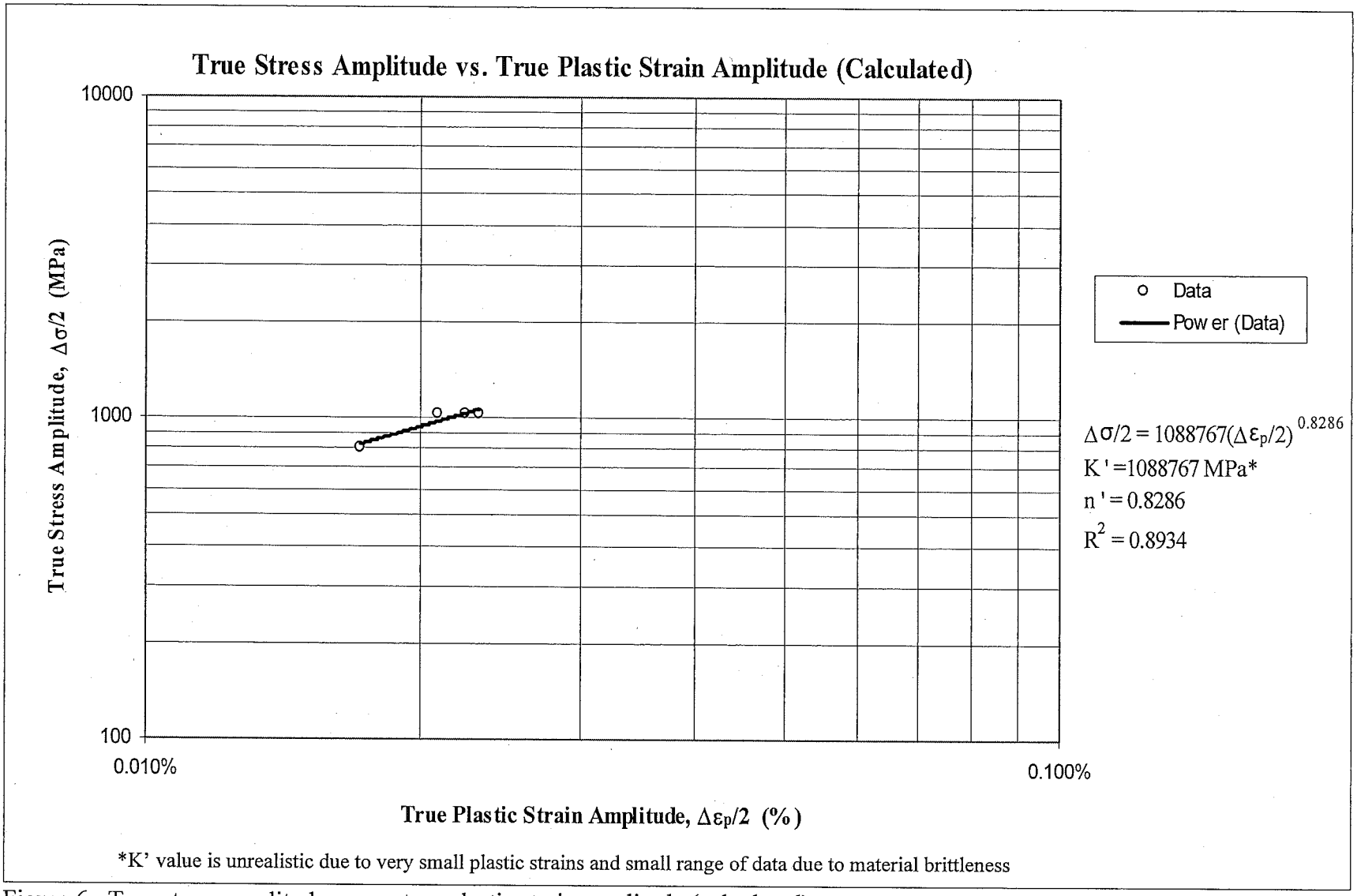

*K' value is unrealistic due to very small plastic strains and small range of data due to material brittleness

Figure 6: True stress amplitude versus true plastic strain amplitude (calculated)

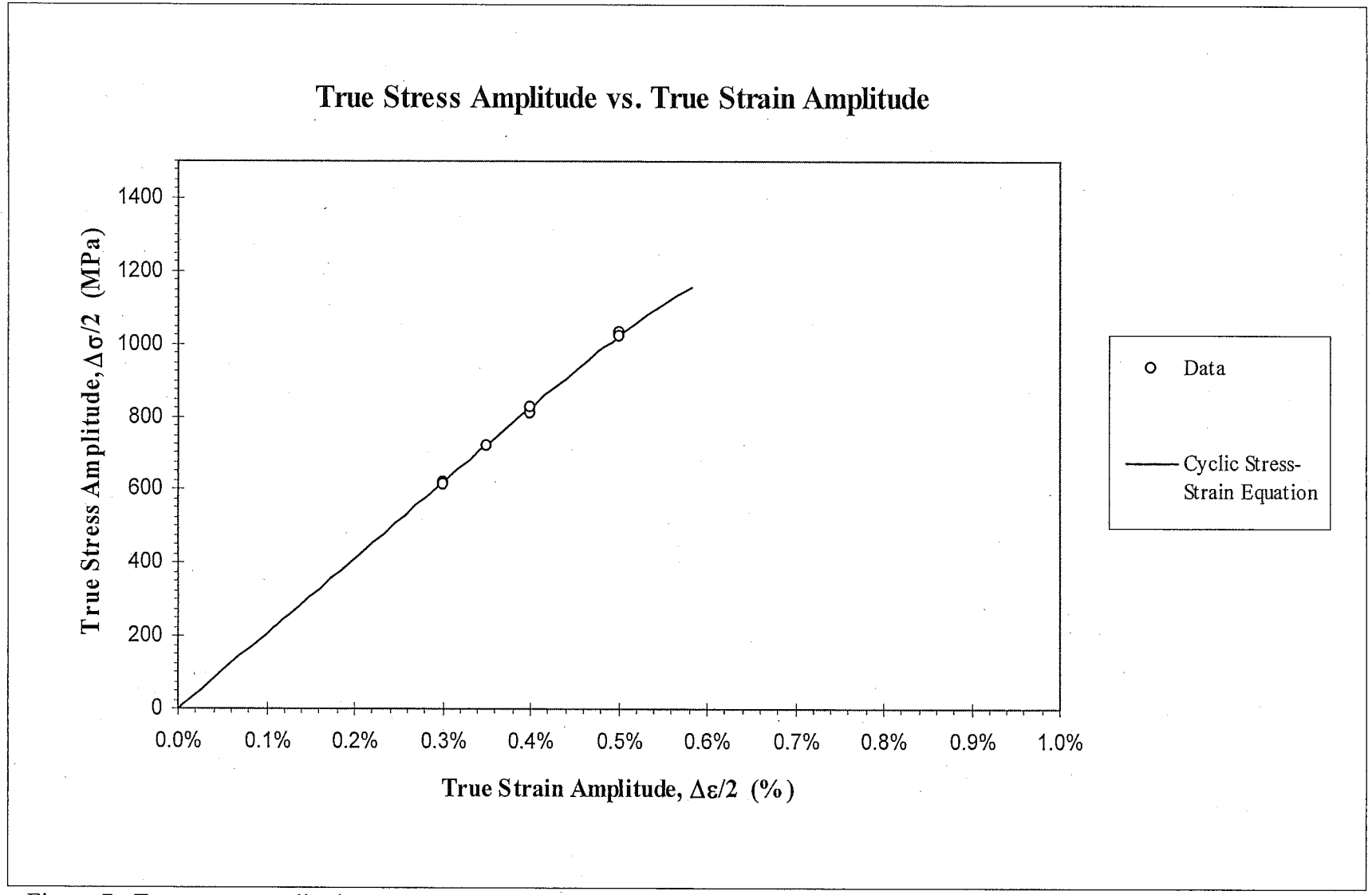

Figure 7: True stress amplitude versus true strain amplitude

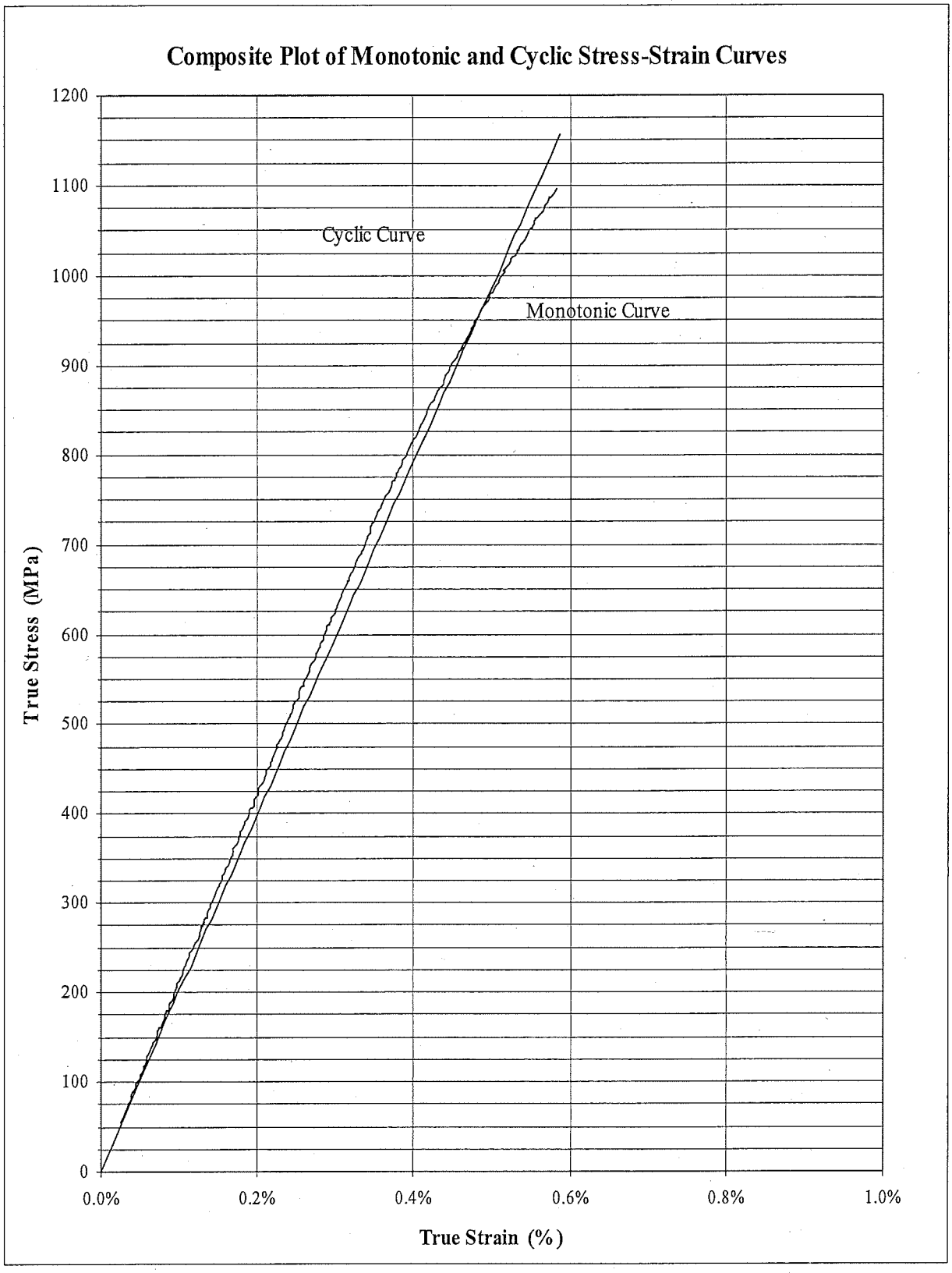

Figure 8: Composite plot of cyclic and monotonic stress-strain curves

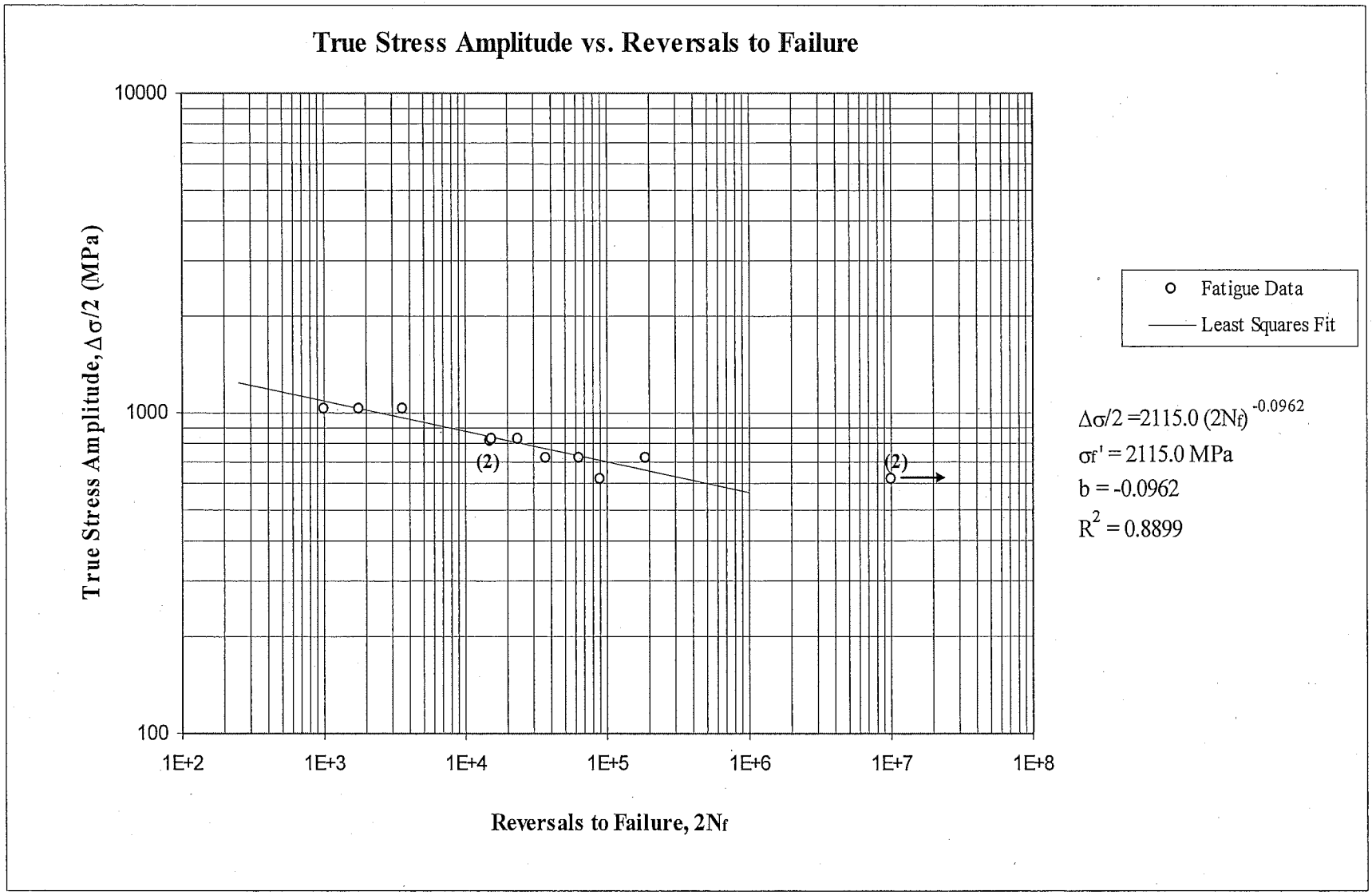

Figure 9: True stress amplitude versus reversals to failure

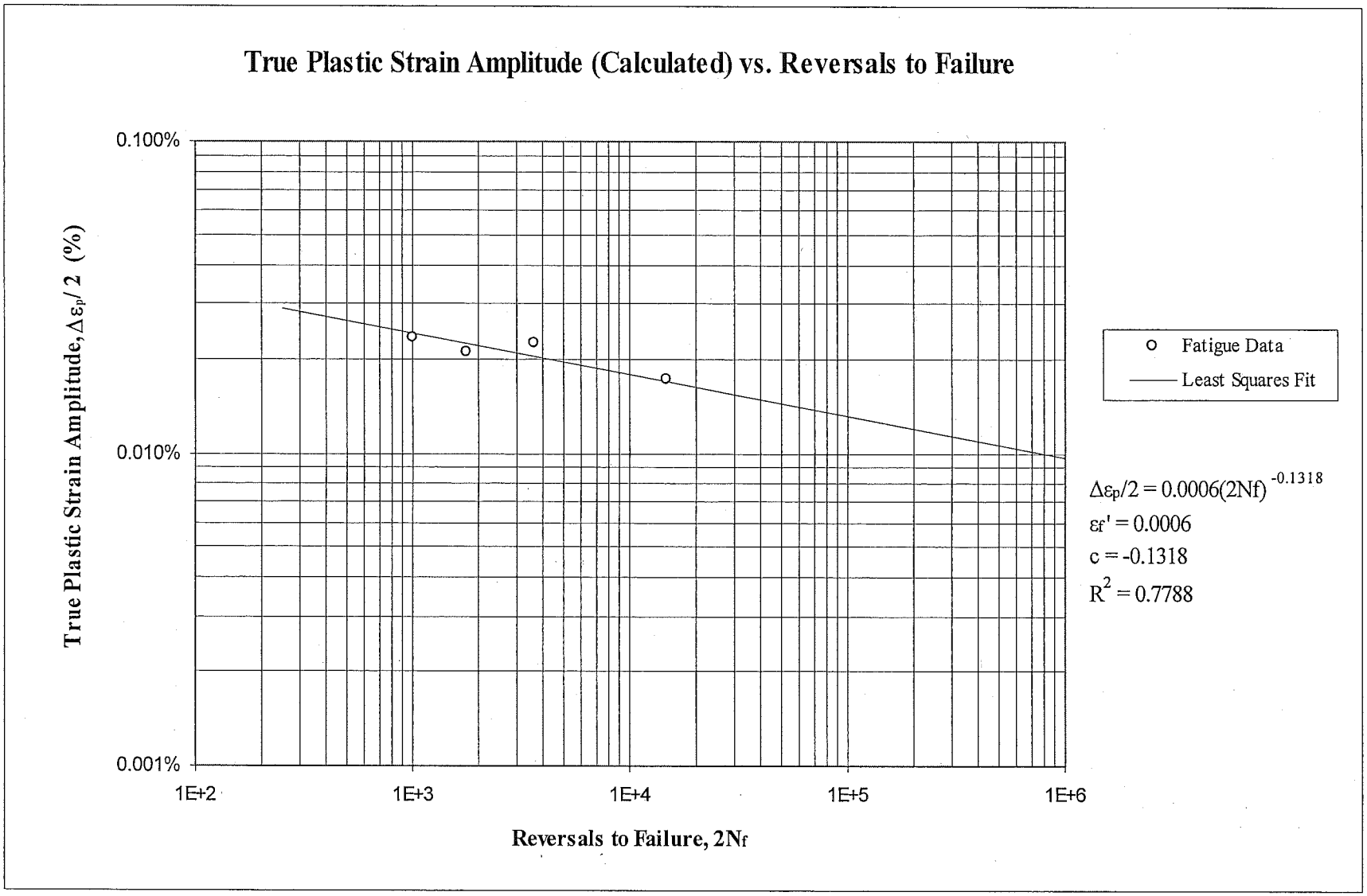

Figure 10: True plastic strain amplitude (calculated) versus reversals to failure

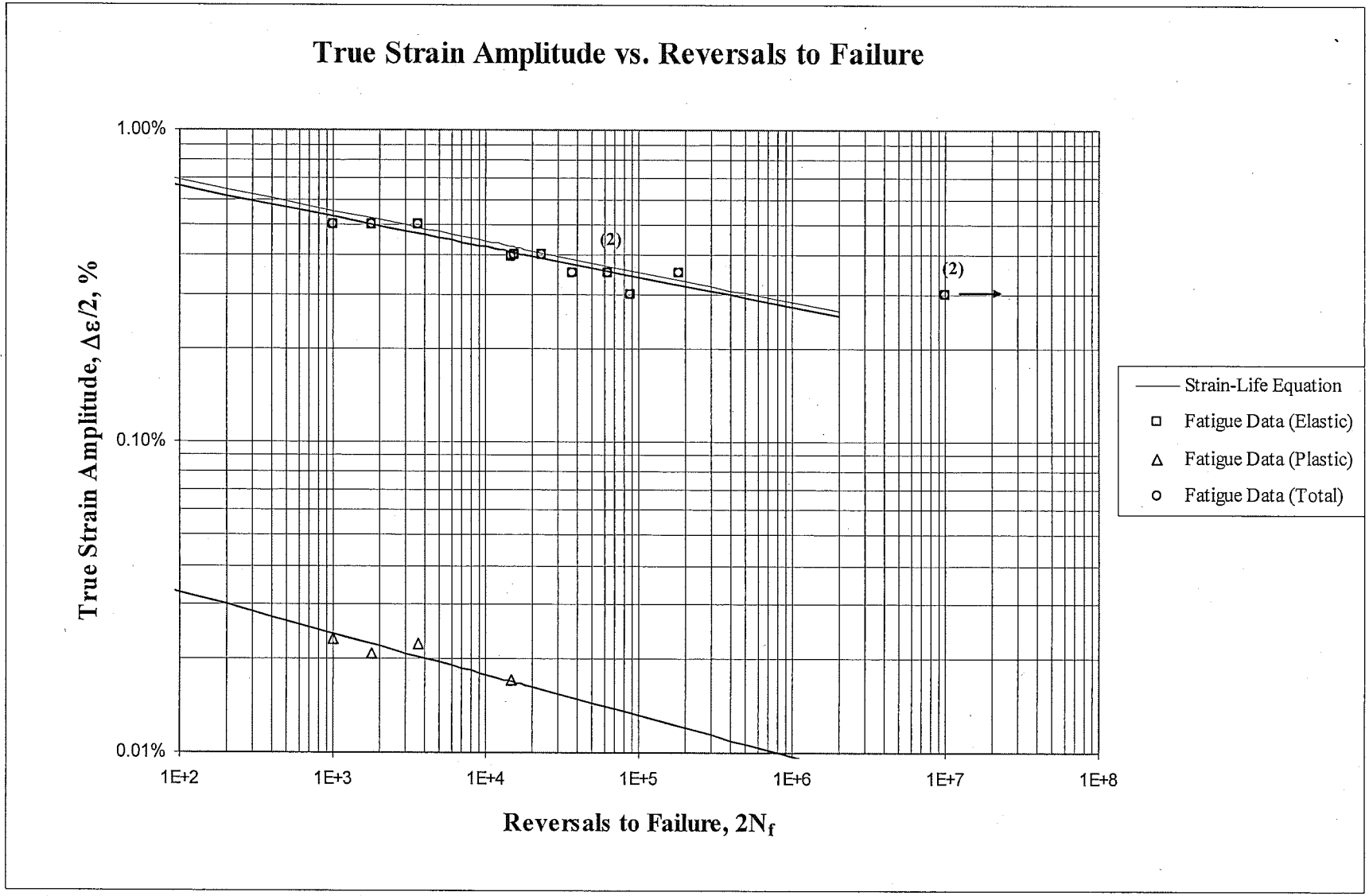

Figure 11: True strain amplitude versus reversals to failure

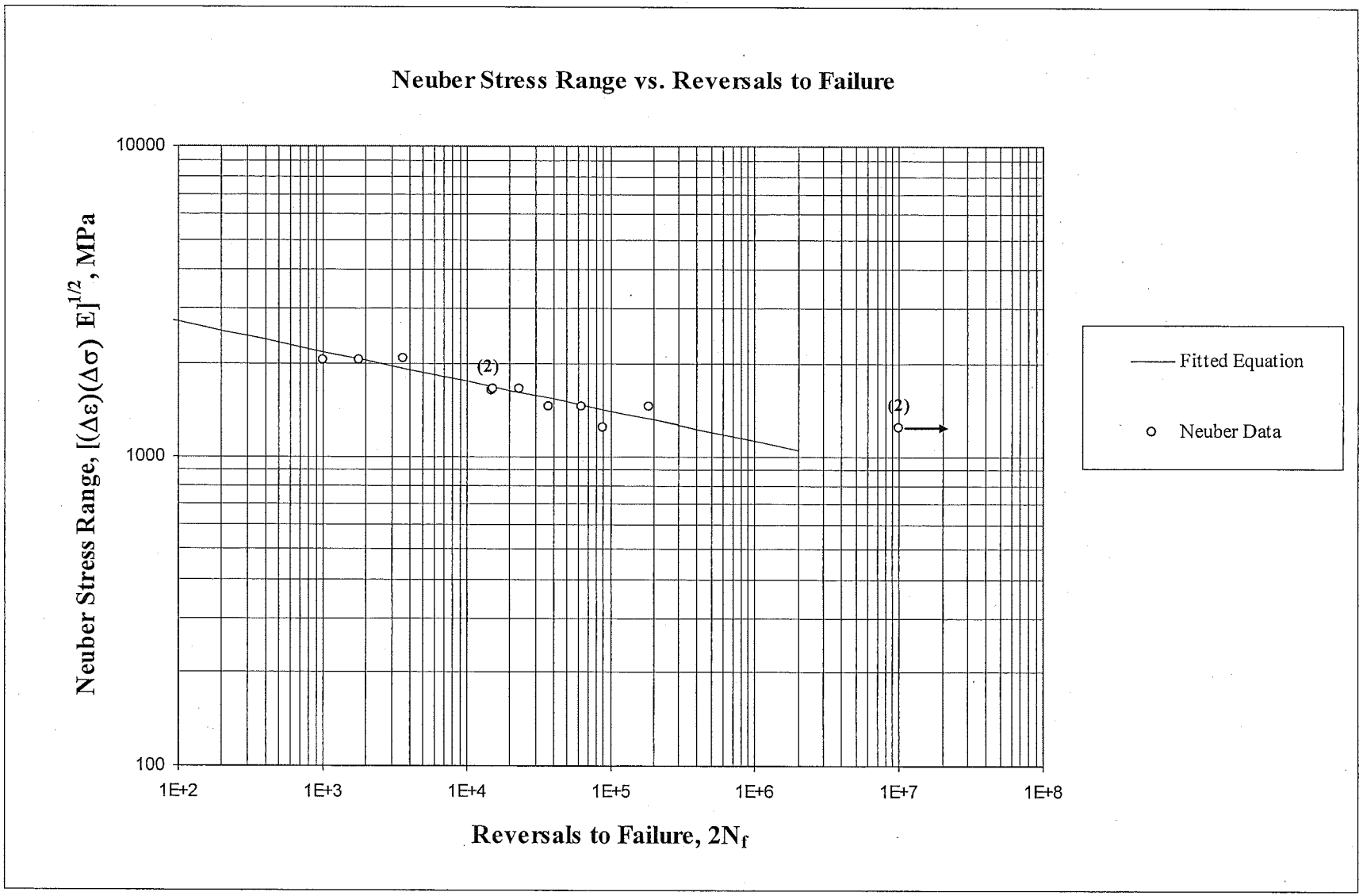

Figure 12: Neuber stress range versus reversals to failure

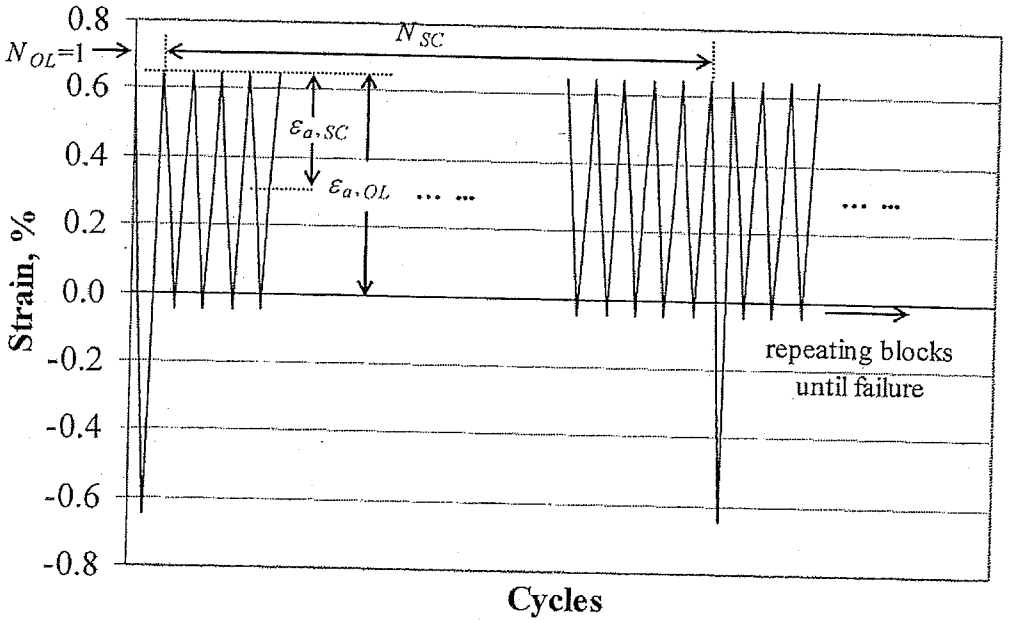

Figure 13: Periodic overload history

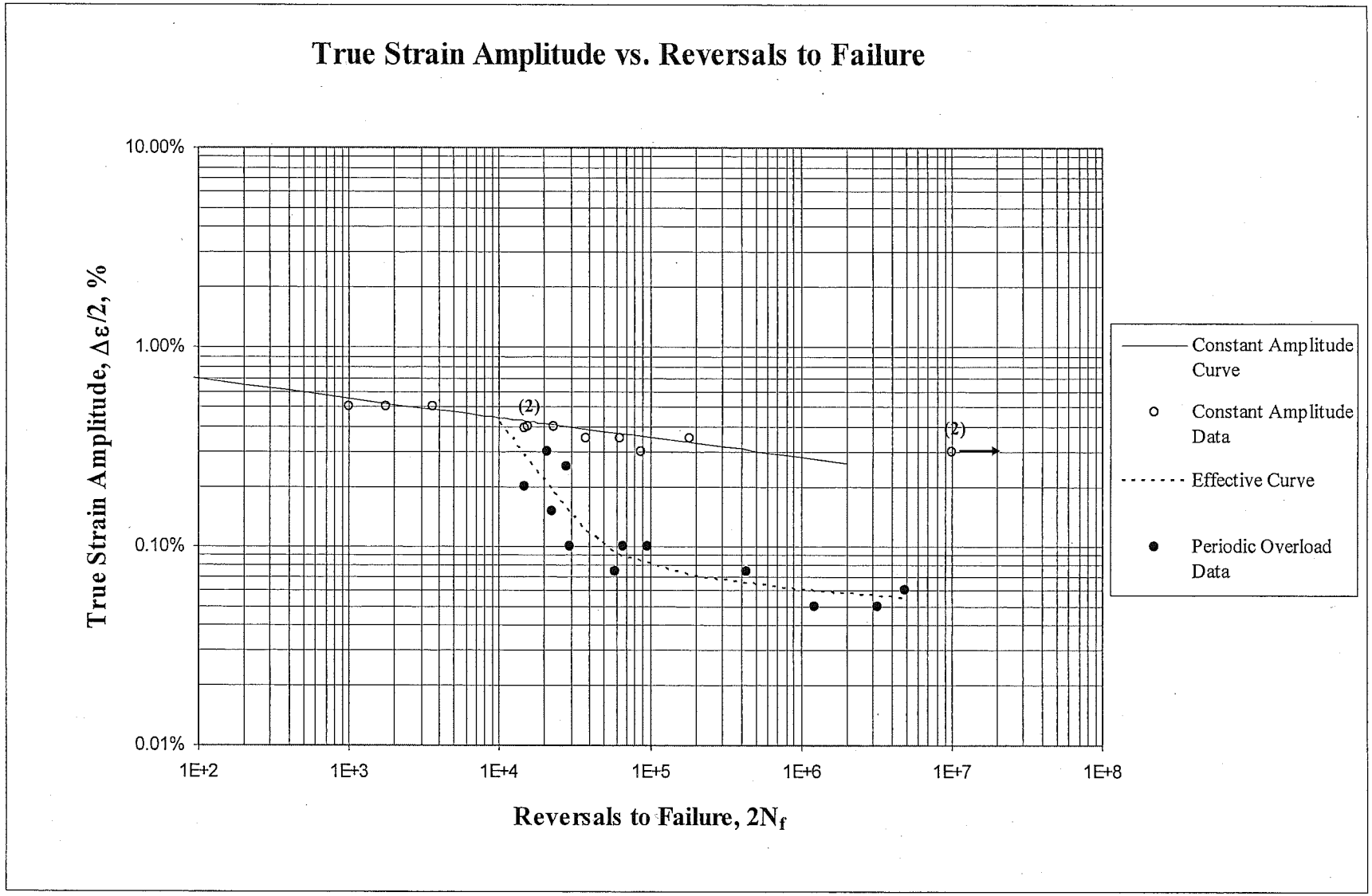

Figure 14: Periodic overload data superimposed with constant amplitude fatigue data

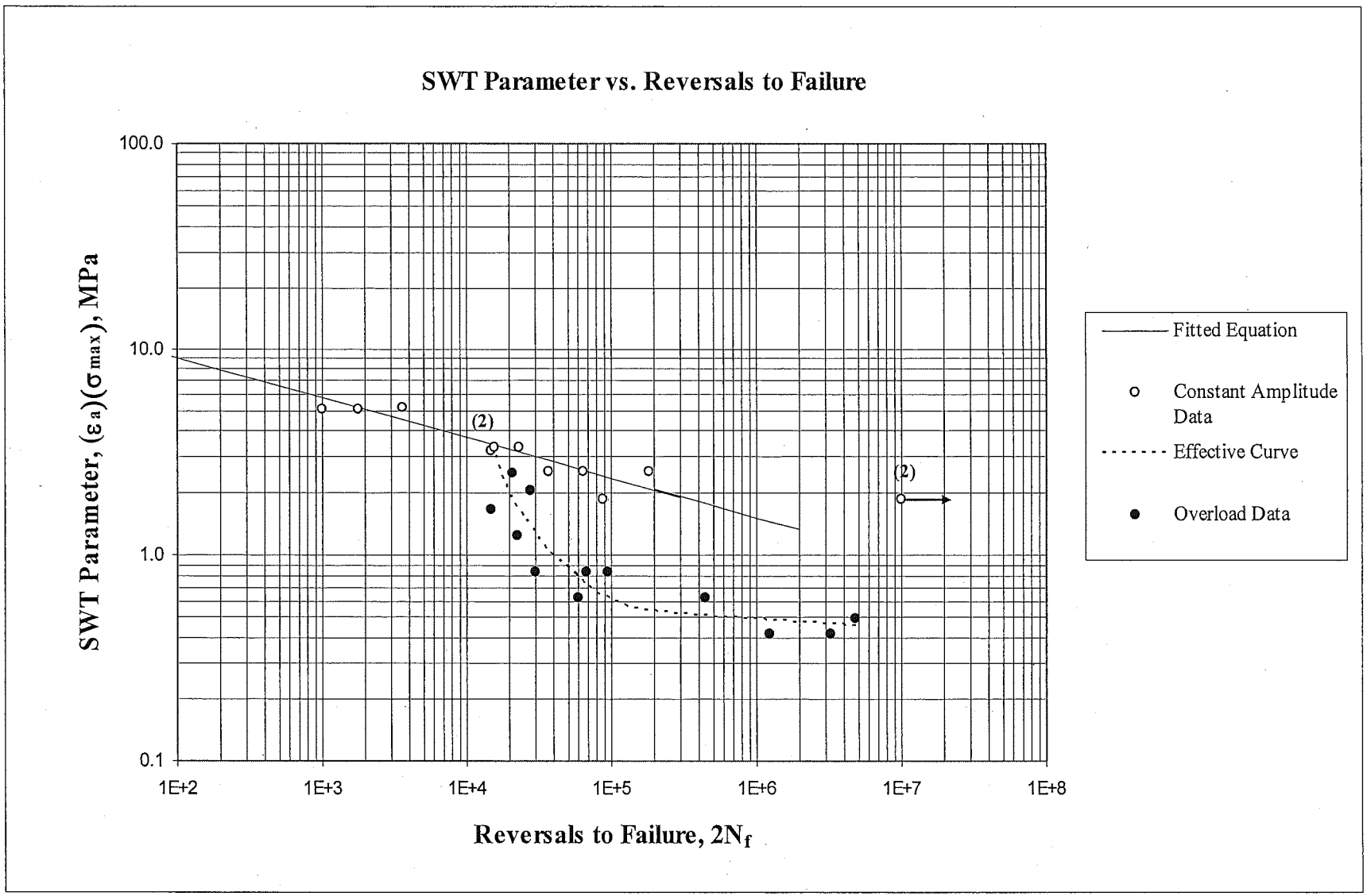

Figure 15: SWT parameter versus reversals to failure. Periodic overload data superimposed on constant amplitude data

REFERENCES

[1] ASTM Standard E606-92, "Standard Practice for Strain-Controlled Fatigue Testing," Annual Book of ASTM Standards, Vol. 03.01, 2004, pp. 593-606.

[2] ASTM Standard E83-02, "Standard Practice for Verification and Classification of Extensometers," Annual Book of ASTM Standards, Vol. 03.01, 2004, pp. 232-244.

[3] ASTM Standard E1012-99, "Standard Practice for Verification of Specimen Alignment Under Tensile Loading," Annual Book of ASTM Standards, Vol. 03.01, 2004, pp. 763-770.

[4] ASTM Standard E8-04, "Standard Test Methods for Tension Testing of Metallic Materials," Annual Book of ASTM Standards, Vol. 03.01, 2004, pp. 62-85.

[5] ASTM Standard E739-91, "Standard Practice for Statistical Analysis of Linear or Linearized Stress-Life (S-N) and Strain-Life (ε-N) Fatigue Data," Annual Book of ASTM Standards, Vol. 03.01, 1995, pp. 670-676.

[6] ASTM Standard E646-00, "Standard Test Method for Tensile Strain-Hardening Exponents (n-values) of Metallic Sheet Materials," Annual Book of ASTM Standards, Vol. 03.01, 2004, pp. 619-626.

[7] Stephens R. I., Fatemi A., Stephens R. R. and Fuchs H. O., "*Metal Fatigue in Engineering*", Second edition, Wiley Interscience, 2000.

Appendix A

Table A.1: Summary of monotonic tensile test results

Specimen ID	D_o, mm (in)	D_f, mm (in)	L_o, mm (in)	L_f, mm (in)	E, Gpa (ksi)	YS (offset=0.2 %), Mpa (ksi)	UYS, Mpa (ksi)	LYS, Mpa (ksi)	YPE, %	S_u, Mpa (ksi)	K, Mpa (ksi)	n	%EL	%RA	ε_f, %	σ_f, Mpa (ksi)
101_11	5.169 (0.2035)	5.169 (0.2035)	7.620 (0.3000)	7.62 (0.3000)	214.7 (31,139)	-	-	-	-	1074.6 (155.9)	1950.7 (282.9)	0.0807	-	-	-	1074.6 (155.9)
101_18	5.169 (0.2035)	5.169 (0.2035)	7.620 (0.3000)	7.62 (0.3000)	214.6 (31,124)	-	-	-	-	1089.7 (158.0)	1778.2 (257.9)	0.0624	-	-	-	1089.7 (158.0)
Average Values					214.7 (31,131)	-	-	-	-	1082.2 (157.0)	1864.5 (270.4)	0.0716	-	-	-	1082.2 (157.0)

Table A.2: Summary of constant amplitude completely reversed fatigue test results

Specimen ID	Test control mode	Test freq., Hz	E, GPa (ksi) [e]	At midlife ($N_{50\%}$)							$(2N_f)_{10\%}$, [b] reversals	$(2N_f)_{50\%}$, [c] reversals	Failure location [d]
				E', GPa (ksi)	$\Delta\varepsilon/2$, %	$\Delta\varepsilon_p/2$ (calculated), %	$\Delta\varepsilon_p/2$ (measured), %	$\Delta\sigma/2$, MPa (ksi)	σ_m, MPa (ksi)	$2N_{50\%}$, [a] reversals			
101_04	strain	1.0	203.8 (29,552)	203.4 (29,496)	0.498%	0.021%	-	1023.8 (148.5)	-73.2 -10.6	1,024	-	1,774	IGL
101_05	strain	1.0	208.1 (30,181)	202.8 (29,412)	0.501%	0.022%	-	1033.0 (149.8)	-75.2 -10.9	2,048	-	3,640	IGL
101_38	strain	1.0	205.6 (29,819)	200.9 (29,141)	0.500%	0.023%	-	1022.4 (148.3)	13.0 1.9	512	-	1,008	IGL
101_02	strain Load	1.3 5.0	206.9 (30,000)	203.7 (29,546)	0.394%	0.017%	-	810.4 (117.5)	92.1 13.4	1,160	-	14,758	IGL
101_13	Load	5.0	-	-	0.400%	0.000%	-	824.9 (119.6)	0.0 0.0	8,192	-	23,206	IGL
101_20	Load	5.0	-	-	0.400%	0.000%	-	824.9 (119.6)	0.0 0.0	8,192	-	15,482	IGL
101_10	Load	10.0	-	-	0.350%	0.000%	-	721.7 (104.7)	0.0 0.0	32,768	-	63,756	IGL
101_15	Load	5.0	-	-	0.350%	0.000%	-	722.1 (104.7)	0.0 0.0	65,536	-	184,368	IGL
101_26	Load	10.0	-	-	0.350%	0.000%	-	721.7 (104.7)	0.0 0.0	16,384	-	37,324	IGL
101_23	Load	24.0	-	-	0.300%	0.000%	-	615.4 (89.3)	0.0 0.0	32,768	-	88,170	IGL
101_14	Load	24.0	-	-	0.300%	0.000%	-	618.7 (89.7)	0.0 0.0	-	-	>5,000,000	No Failure
101_16	Load	24.0	-	-	0.300%	0.000%	-	618.4 (89.7)	0.0 0.0	-	-	>5,000,000	No Failure

[a] $2N_{50\%}$ is defined as the midlife reversal ; [b] $2(N_f)_{10\%}$ is defined as reversal of 10% load drop

[c] $2(N_f)_{50\%}$ is defined as reversal of 50% load drop or failure

[d] IGL = Inside gage length;

[e] E value was calculated from the first cycle

Table A.3: Summary of the periodic overload fatigue test results

Spec. ID	Test Control Mode	Test Freq. OL/SC (Hz)	E (GPa) [b]	Load history Description												Exp. Life (Blks)	$N_{f,sc(eq)}$ (Cycles)	OL Damage Ratio	Failure Location [a]
				$\varepsilon_{a,SC}$ (%)	$\varepsilon_{m,SC}$ (%)	$\Delta\varepsilon_p/2_{,SC}$ (calculated) (%)	$\sigma_{a,SC}$ (MPa)	$\sigma_{m,SC}$ (MPa)	N_{SC} (Cycles)	$\varepsilon_{a,OL}$ (%)	$\Delta\varepsilon_p/2_{,OL}$ (calculated) (%)	$\sigma_{a,OL}$ (MPa)	$\sigma_{m,OL}$ (MPa)	$N_{f,OL}$ (Cycles)				
101_07	Load	2 / 10	-	0.300%	0.100%	0.000%	618.4	206.0	100	0.400%	0.000%	824.4	0.0	10,000	103	10,407	0.010	IGL
101_21	Load	2 / 10	-	0.250%	0.150%	0.000%	515.4	309.0	100	0.400%	0.000%	824.4	0.0	10,000	137	13,890	0.014	IGL
101_24	Load	2 / 10	-	0.200%	0.200%	0.000%	412.3	411.8	100	0.400%	0.000%	824.1	0.0	10,000	74	7,455	0.007	IGL
101_22	Load	2 / 10	-	0.150%	0.250%	0.000%	309.1	515.1	100	0.400%	0.000%	824.1	0.0	10,000	112	11,327	0.011	IGL
101_32	Load	2 / 10	-	0.100%	0.300%	0.000%	206.0	618.4	50	0.400%	0.000%	824.4	0.0	10,000	288	14,827	0.029	IGL
101_25	Load	2 / 10	-	0.100%	0.300%	0.000%	206.1	618.0	50	0.400%	0.000%	824.1	0.0	10,000	629	33,561	0.063	IGL
101_08	Load	2 / 10	-	0.100%	0.300%	0.000%	206.1	618.0	100	0.400%	0.000%	824.1	0.0	10,000	458	47,998	0.046	IGL
101_35	Load	2 / 10	-	0.075%	0.325%	0.000%	154.6	669.8	100	0.400%	0.000%	824.4	0.0	10,000	286	29,442	0.029	IGL
101_09	Load	2 / 10	-	0.075%	0.325%	0.000%	154.2	670.1	100	0.400%	0.000%	824.3	0.0	10,000	1,802	219,810	0.180	IGL
101-27	Load	2 / 10	-	0.060%	0.340%	0.000%	123.5	700.9	300	0.400%	0.000%	824.4	0.0	10,000	4,479	2,433,798	0.448	IGL
101_31	Load	2 / 10	-	0.050%	0.350%	0.000%	102.9	721.4	100	0.400%	0.000%	824.4	0.0	10,000	3,806	614,466	0.381	IGL
101 06	Load	2 / 10	-	0.050%	0.350%	0.000%	103.0	721.1	300	0.400%	0.000%	824.1	0.0	10,000	3,516	1,626,774	0.352	IGL

[a] IGL = Inside gage length

[b] E value was calculated from the first cycle

All stress values reported are from mid-life

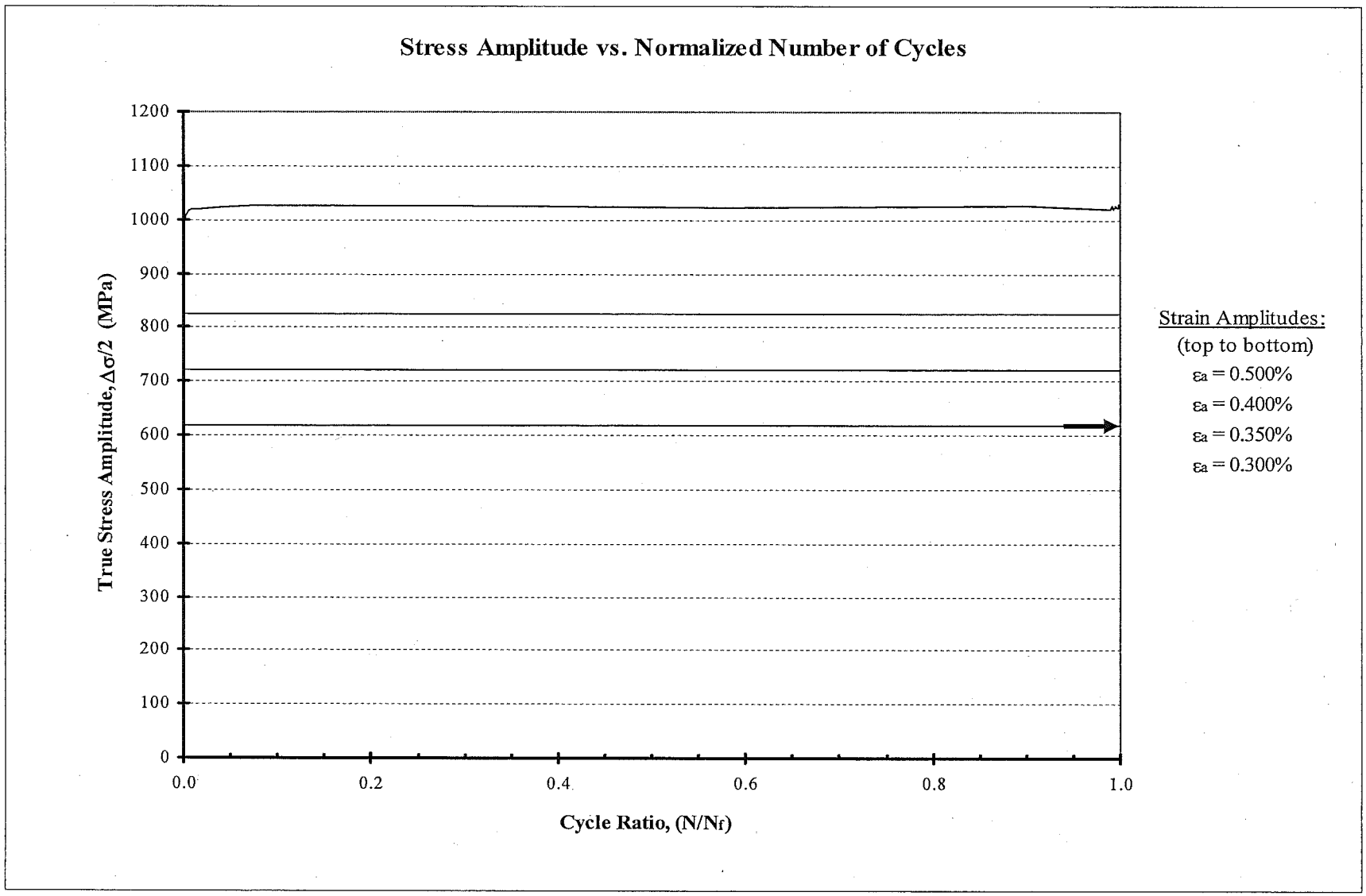

Figure A.1a: True stress amplitude versus normalized number of cycles

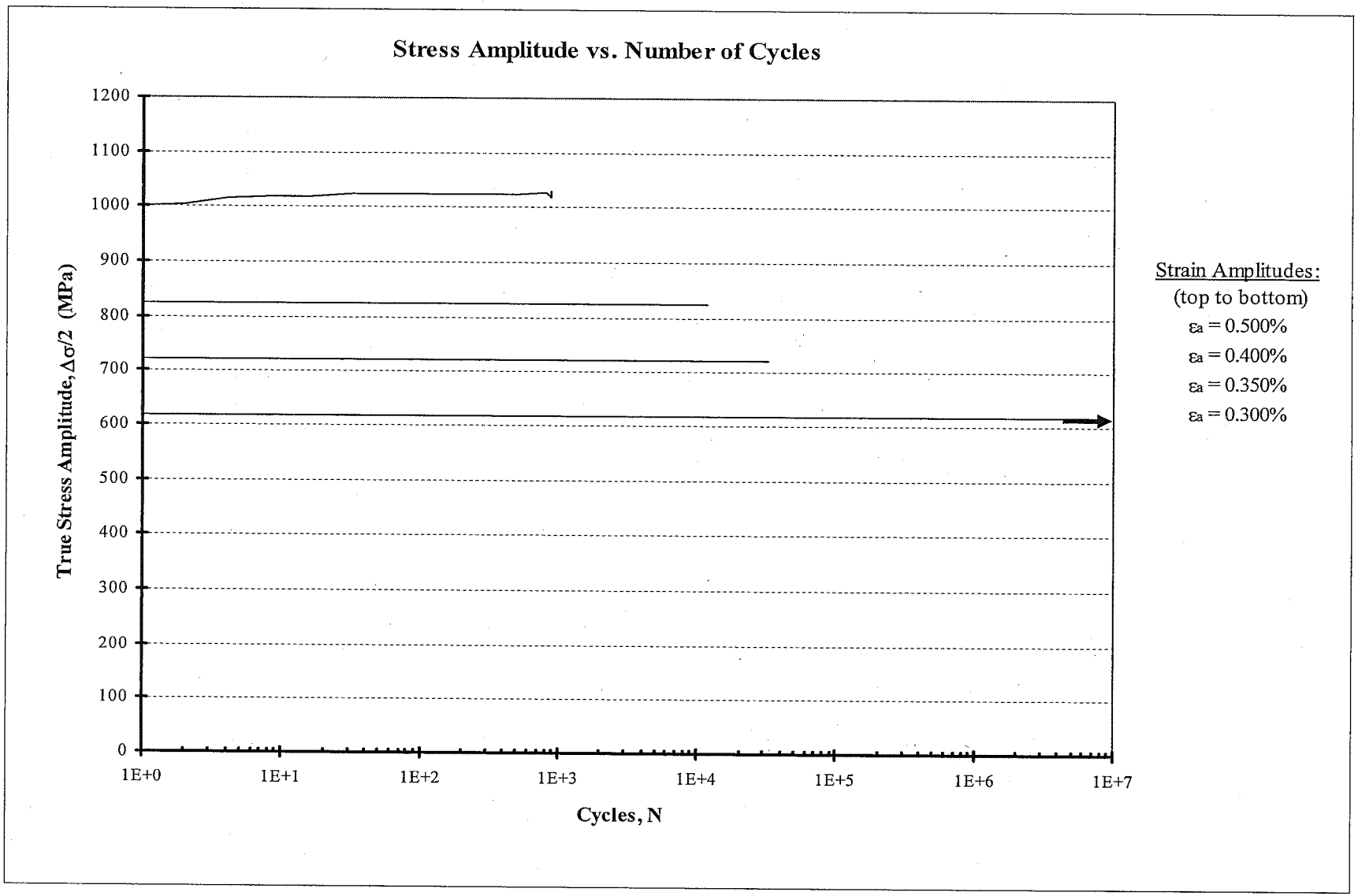

Figure A.1b: True stress amplitude versus number of cycles

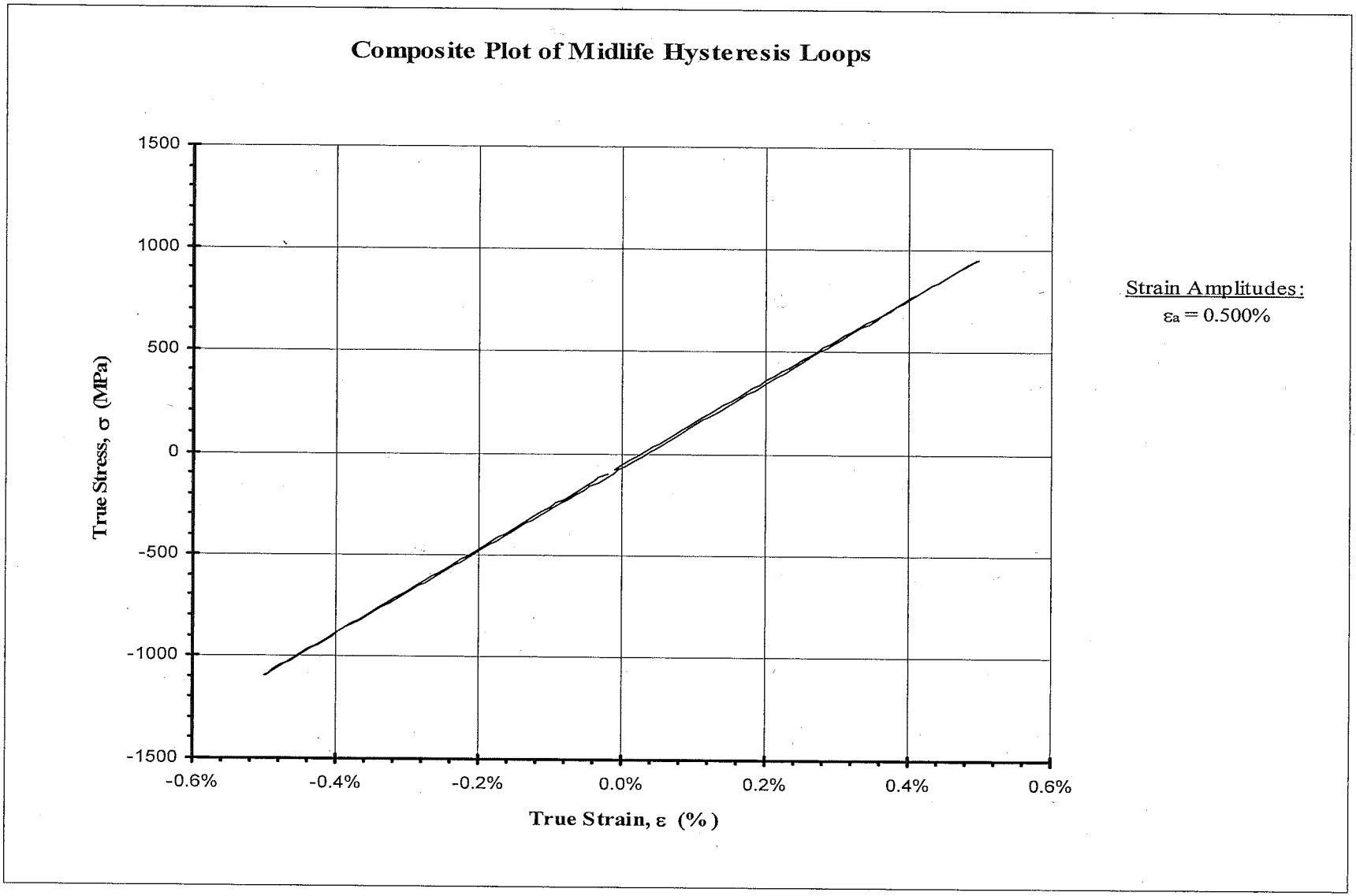

Figure A.2: Composite plot of midlife hysteresis loops

Appendix B

CHRYSLER
UAW - Chrysler
SCIENTIFIC LABS & PROVING GROUNDS

Materials Engineering Lab Report

LTR Number: 133873

To: Peter Bauerle **Phone:** 776-7387
Location: CTC

From: Metallography **Completed:** 12/17/2008
Chemistry - XRay
Mechanical Properties

Subject/Part Name: Fatigue Specimen-Iteration 101/105
Report Status: Complete
Originator: Peter Bauerle
Originator Phone: 248-576-7387
Number of Parts: 1
Nature of Work: Pilot, Mule, Program Development Issue
Vendor:
Plant:
P/N:
MS:
PS:

History of Part

The samples represent fatigue specimens that will be tested by AISI. The specimens have been prepared from an 8822 steel with low side hardenability. The sample has been through carburized in the gage section by austenitizing at 1700F with a 0.9% carbon potential prior to quenching in 150F oil and then tempering at 425F to an aim hardness of 58-60 HRC.

Test Results

Metallography - 133873

General Microstructure Description (Performed By: Gerry Shulke)

The mounted sample was reground and polished. The sample was examined using light microscopy. The surface of the sample contained roughly 28 microns of intergranular oxidation. The sample was then etched with 3% nital and was reexamined. The microstructure of the case was tempered martensite with retained austenite. The amount of retained austenite was estimated to be 9.1% using image analysis. The microstructure of the core was tempered martensite.

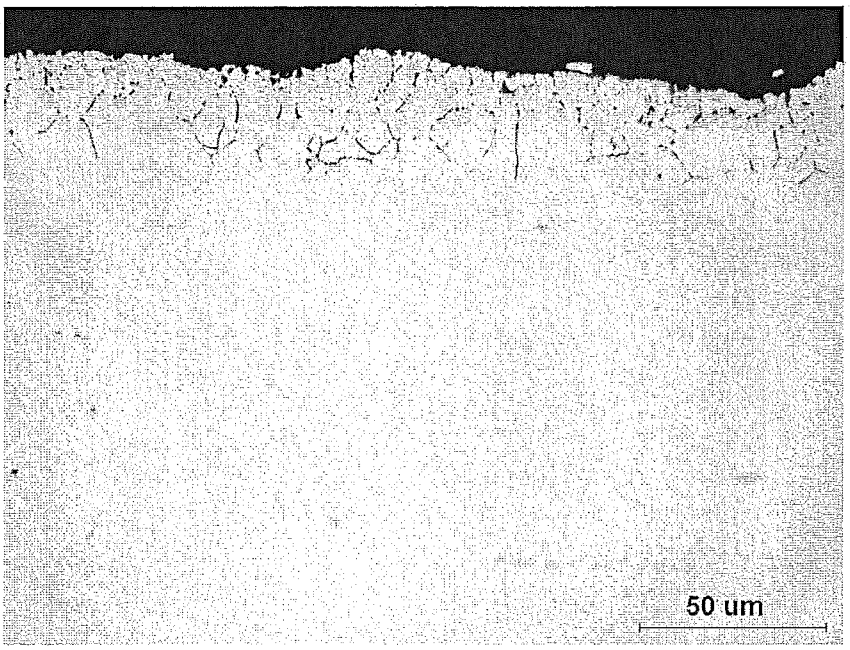

Figure Met1. Image of the surface of the grip end in the unetched condition showing the intergranular oxidation.

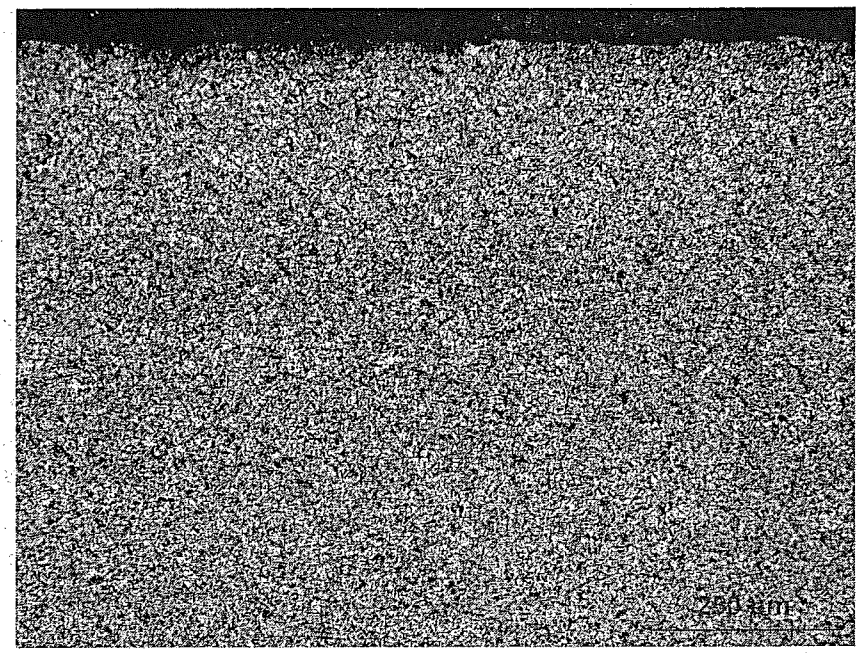

Figure Met2. Medium magnification image of the surface fo the grip end.

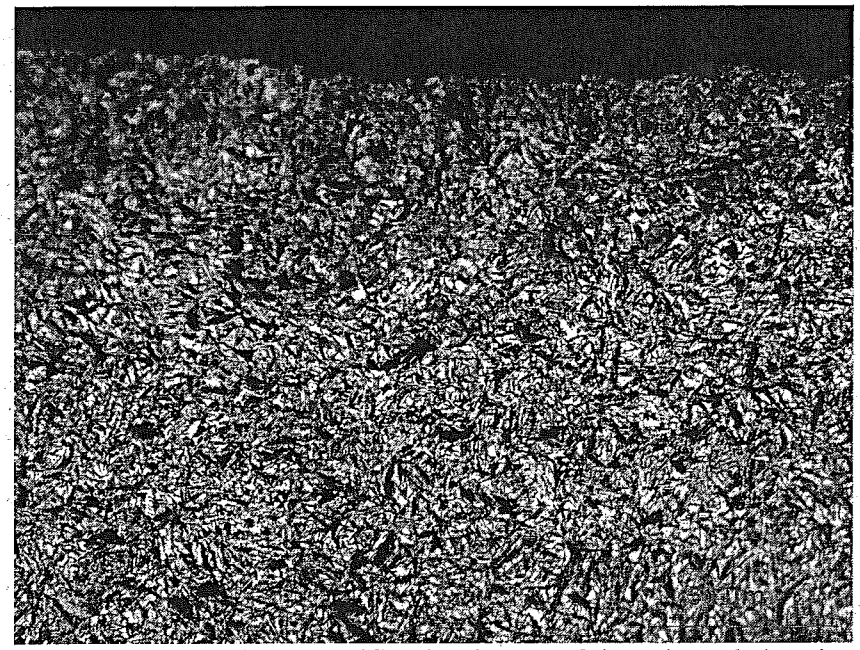
Figure Met3. Higher magnification image of the grip end showing retained austenite and tempered martensite.

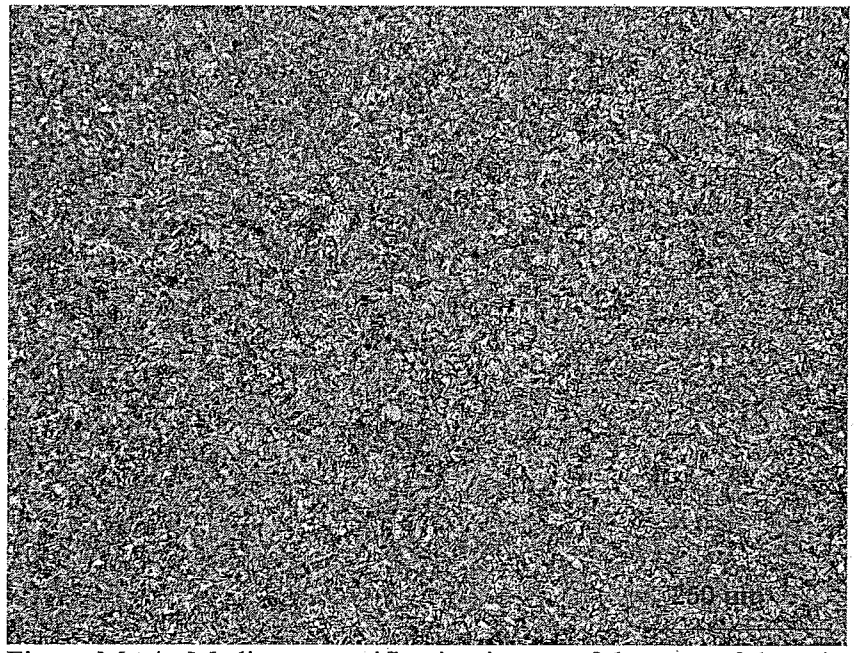

Figure Met4. Medium magnification image of the core of the grip end.

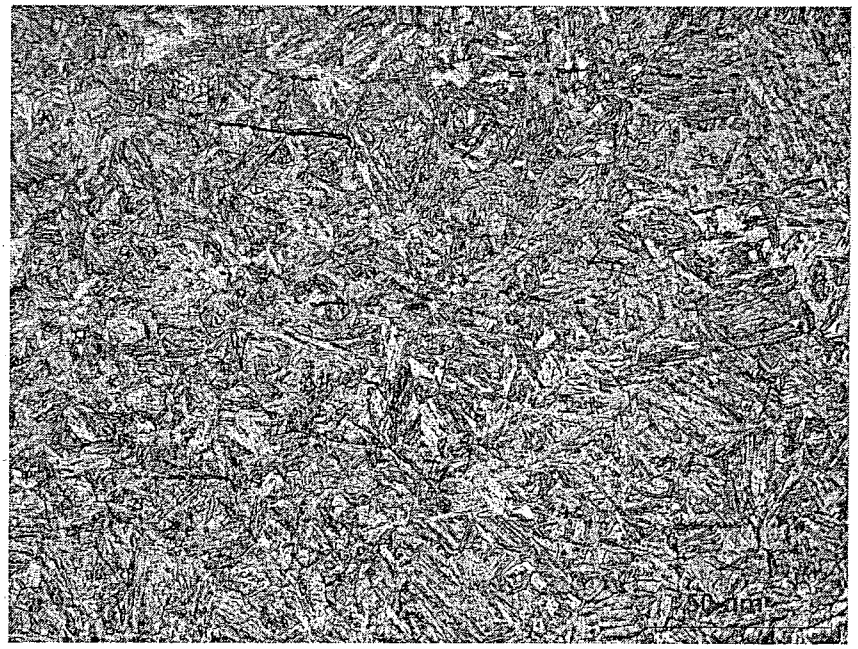

Figure Met5. Higher magnification image of the microstructure of the core of the grip end showing tempered martensite.

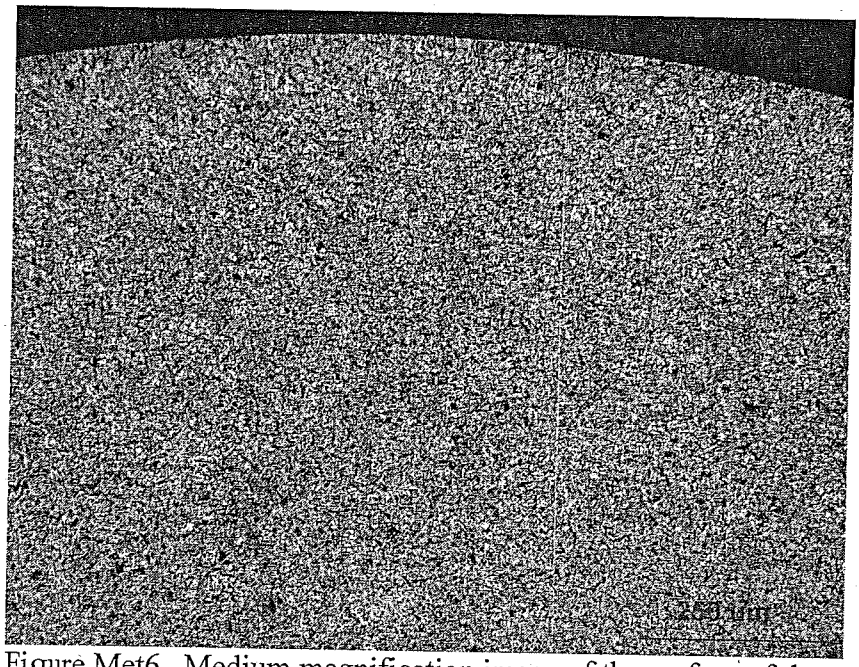

Figure Met6. Medium magnification image of the surface of the gage section.

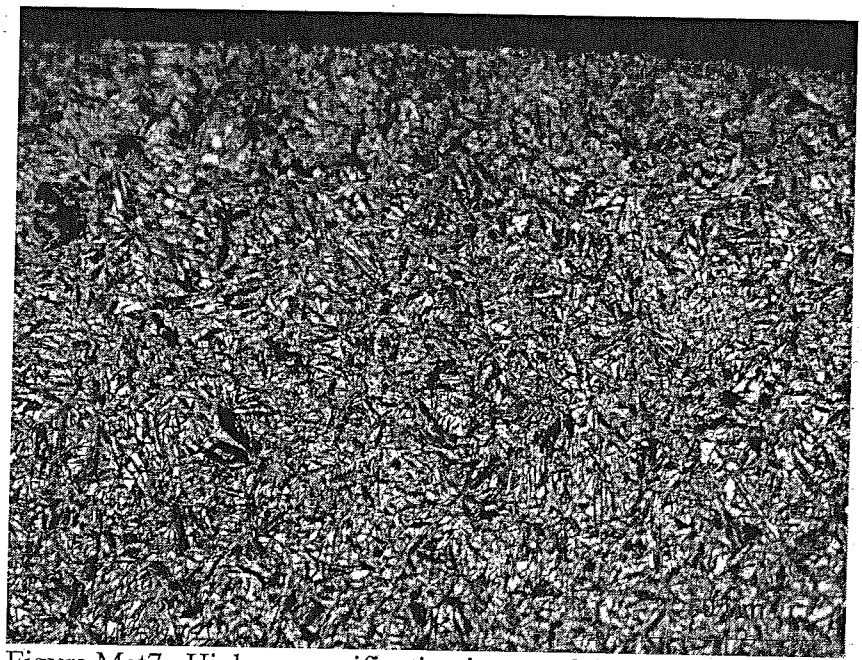

Figure Met7. Higher magnification image of the surface of the gage section showing tempered martensite and retained austenite.

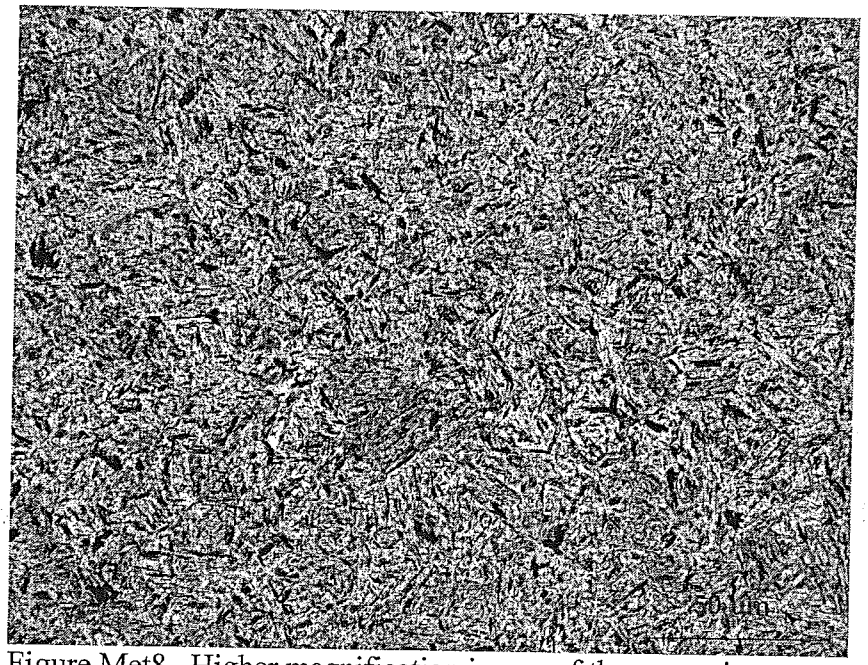

Figure Met8. Higher magnification image of the core microstructure of tempered martensite in the core of the gage section.

Mechanical Properties - 133873

Hardness - Rockwell (Performed By: Greg Cornelissen)

Grip end (surface hardness) - 59.7 HRC 59.5 HRC 59.0 HRC

Hardness - Micro (Performed By: Greg Cornelissen)

Newage Microhardness Tester - 1000gf

Microhardness traverse starting from the edge of the part.

.005"	59.4 HRC
.010"	59.9 HRC
.015"	59.2 HRC
.020"	57.9 HRC
.025"	59.8 HRC
.030"	59.6 HRC
.040"	58.0 HRC
.050"	57.2 HRC
.060"	55.1 HRC
.070"	55.7 HRC
.080"	55.5 HRC
.090"	55.8 HRC
.100"	55.9 HRC